CONTENTS

PUBLICATION POLICY

The *ECMWF Newsletter* is published quarterly. Its purpose is to make users of ECMWF products, collaborators with ECMWF and the wider meteorological community aware of new developments at ECMWF and the use that can be made of ECMWF products. Most articles are prepared by staff at ECMWF, but articles are also welcome from people working elsewhere, especially those from Member States and Co-operating States. The *ECMWF Newsletter* is not peer-reviewed.

Editor: Bob Riddaway

Typesetting and Graphics: Rob Hine

Any queries about the content or distribution of the *ECMWF Newsletter* should be sent to Bob.Riddaway@ecmwf.int

Guidance about submitting an article is available at www.ecmwf.int/publications/newsletter/guidance.pdf

CONTACTING ECMWF

Shinfield Park, Reading, Berkshire RG2 9AX, UK

Fax: . . . . . +44 118 986 9450

Telephone: National 0118 949 9000

International . . . . . +44 118 949 9000

ECMWF website . . . . . http://www.ecmwf.int

Assessing uncertainty in analyses and forecasts

In the spring 2010 edition of the ECMWF Newsletter the editorial describes the new ECMWF convention that came into force in June 2010. In the same edition the new ensemble based data assimilation system (EDA) and its impacts on the probabilistic forecasting system (EPS) were described in two articles. The new EDA system was introduced in operations in June, almost at the same time as the new convention came into force. Both events will impact the future of ECMWF and this editorial focuses on the future potential of EDA.

The uncertainty in the initial state is one of the factors that limits the accuracy of weather forecasts; model uncertainty is the other main factor. Both uncertainties can be taken into account by using an ensemble method for initial state and model perturbations. The ECMWF atmospheric prediction system includes both deterministic and probabilistic components.

- The deterministic model is started from an analysis based on an optimal combination of information gathered from observations and a short-range forecast. It is constructed using a variational technique where the relative uncertainties in the short-range forecast and the observations are used to calculate an optimal combination of the two.
- The probabilistic ensemble forecasts are initialised from a range of initial states around the deterministic analysis. The range of initial states reflects the uncertainty in the analysis. Introducing stochastic perturbations in the model equations allows model uncertainty to be taken into account.

The recently-developed EDA merges the variational data assimilation and ensemble prediction techniques. EDA provides initial state uncertainty estimates that are dependent on the flow of the day. Close to fronts and rapidly developing cyclones the uncertainties are larger than around a stable anticyclone. This information can both be used to increase the weights given to observations in the variational analysis and to provide a flow-dependent initial state uncertainty in the EPS. Rapidly developing cyclones are generally more difficult to predict, so a realistic estimate of the analysis error around the cyclones will improve the performance of probabilistic predictions. In particular it will give a reliable estimate of risks for heavy precipitation, strong winds and other phenomena associated with severe weather events.

The present implementation of EDA is only used to give initial state perturbations for the EPS. Future versions of EDA will also provide feedback to the variational analysis. As a result the background error estimation in flow situations with rapidly developing cyclones and in the tropics will improve considerably. In addition, probabilistic products such as strike probabilities for storms are expected to become much more reliable.

In this issue of the ECMWF Newsletter Lizzie Froude shows how well cyclone track probabilities are captured by currently available ensemble prediction systems around the world – we can expect further improvements in the future.

Another advantage of EDA is the possibility to provide space and time dependent analysis error estimates. These will be an important part of future reanalyses over periods where the observation coverage is limited and variable, such as in the first half of the twentieth century. Finally EDA is well adapted to future computer architectures as it scales very well on massively parallel computing systems.

Erland Källén

New items on the ECMWF website

ANDY BRADY

Workshop on Non-hydrostatic Modelling

The workshop was held on 8–10 November 2010 and brought together leading experts in the field of non-hydrostatic modelling to discuss recent developments in this area and to provide recommendations on how to prepare ECMWF's Integrated Forecasting System (IFS) for global atmospheric modelling at future high to ultra-high resolutions.

- http://www.ecmwf.int/newsevents/meetings/workshops/2010/Non_hydrostatic_Modelling/

Model versus climate comparison charts

The climate of the ECMWF model is compared against observational datasets and reanalysis in terms of mean state and synoptic variability for a list of model cycles from the ERA40 and ERA-Interim cycles to the current operational cycle.

- http://www.ecmwf.int/products/forecasts/d/inspect/catalog/research/physics_clim/

Climate monitoring products using ECMWF reanalysis

ERA is ECMWF's global atmospheric reanalysis of the period 1989 to present. Time series of global 2-metre temperature anomalies, and many other climate indicators produced from ERA-Interim and ERA-40 monthly data. Plots are updated monthly.

- http://www.ecmwf.int/research/era/

Metview version 4

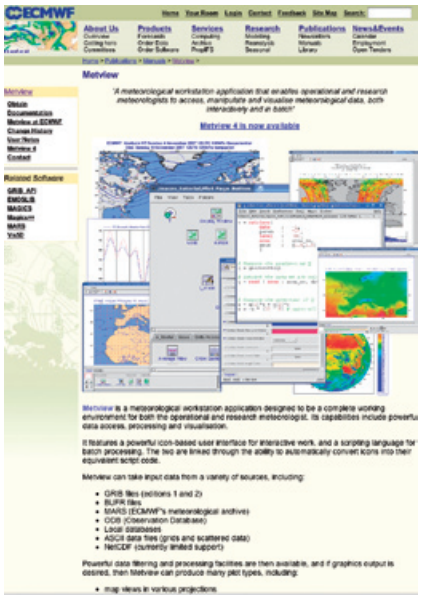

Metview 4 is the latest generation of the Metview meteorological workstation software. This version introduces a new visualisation module based on Magics++. Further, this version now fully supports GRIB 2 throughout. The installation process has been simplified and has support for 64-bit architectures. There is an article about Metview 4 in this edition of the ECMWF Newsletter and more information will be provided in future editions.

- http://www.ecmwf.int/publications/manuals/metview/

14th Workshop on the Use of High Performance Computing in Meteorology

Every second year ECMWF hosts a workshop on the use of high performance computing in meteorology. The emphasis of this workshop was on running meteorological applications at sustained teraflops performance in a production environment. Particular emphasis was placed on the future scalability of NWP codes and the tools and development environments to facilitate this.

- http://www.ecmwf.int/newsevents/meetings/workshops/2010/high_performance_computing_14th/

Changes to the operational forecasting system

DAVID RICHARDSON

New cycle (Cy36r4)

A new cycle of the ECMWF forecast and analysis system, Cy36r4, was implemented on 9 November 2010.

Changes to the deterministic forecasting system

The new cycle includes a new cloud parametrization scheme with five prognostic variables on model levels: cloud fraction, cloud water, cloud ice, rain water content and snow water content. The latter two are new model variables. New surface analysis schemes are introduced for snow and soil moisture.

The main changes included in this cycle are:

- Five-species prognostic microphysics scheme, introducing cloud rain water content, and cloud ice water content as new model variables.
- Retuning and simplification of convective entrainment/detrainment and land/sea dependent threshold for precipitation.
- Retuning of subgrid-scale orographic gravity wave drag.
- Adjustment to diffusion in stable boundary layers near the surface.
- All-sky improvements of microwave radiance assimilation.
- Adaptation to neutral wind of the observation operator for scatterometer data.
- New soil-moisture analysis scheme (SEKF, simplified ensemble Kalman filter).
- New snow analysis based on OI (Optimum Interpolation), and upgrade of NESDIS snow cover data to 4 km resolution.
- Monthly varying climatology of leaf area index (LAI) based on MODIS data.

◆ The 4D-Var of the Early Delivery suite performs two rather than three updates of the outer loop.

The new cycle shows some benefit in terms of objective scores in the medium range in both hemispheres, particularly in the upper troposphere. For winds, the verification against observations is generally positive, whereas verification against analyses tends to be negative in the shorter range, which can be explained by higher variability in the analysed wind fields. The new snow analysis improves several issues that affected the analysed snow depth on the 2009/2010 winter season. Modifications to the stable boundary layer improve the diurnal cycle of 2m temperature, especially some reduction of the night-time cold bias over Europe. The tropospheric humidity analysis has significantly improved.

Changes to the EPS

The main changes to the EPS included in this cycle are:

◆ Revision of stochastically perturbed physical tendencies.

◆ Introduction of spectral stochastic backscatter scheme.

◆ Retuned initial perturbation amplitudes.

The impact of the changes to the EPS are primarily seen in slightly improved probabilistic scores in the extra-tropics, and better tuned spread-skill relationship – especially for 500 hPa geopotential height in the earlier forecast ranges (days 1–5).

More information on changes to the forecasting system can be found at:

◆ www.ecmwf.int/products/data/operational_system/evolution/evolution_2010.html

New web-based data recovery initiatives to support climate reanalysis

DICK DEE

Two recently launched websites allow anyone with access to the Internet to make a fundamental contribution to climate science, by helping to digitise historic weather observations. Please visit '*oldWeather*' at:

◆ http://www.oldweather.org

and '*Data rescue at home*' at:

◆ http://data-rescue-at-home.org

The EU-funded ERA-CLIM project, briefly described in *ECMWF Newsletter No. 123*, will develop the input data sets and assimilation systems needed for a new atmospheric reanalysis of the 20th century. A major challenge for the project is to collect and prepare the observations for the early part of the reanalysis, when a well-coordinated and truly global observing system had not yet developed. Fortunately, vast numbers of weather observations for this period do in fact exist; they can be found in archives at national meteorological services, in local parishes and administrative offices where many of the weather records used to be kept, and in ship logs stored in libraries, museums, and other institutions.

A growing number of local and international efforts are now taking place to recover these valuable data, in response to the need for more accurate observational information about the recent climate. Much of this work is connected with and motivated by climate reanalysis activities such as the pioneering 20th Century Reanalysis Project conducted in the United States. Naturally, before any of the data can actually be used for reanalysis they must first be made available in digital form. This is why a large part of the ERA-CLIM project will be dedicated to data recovery and digitisation work, concentrating on upper-air observations made with early radiosondes and kites, as well as surface weather observations in sparsely observed regions of the globe.

ERA-CLIM is closely linked with the ACRE initiative –

◆ http://www.met-acre.org

which supports and coordinates many data recovery and digitisation projects around the world. The work required to locate, scan, and digitise the data is

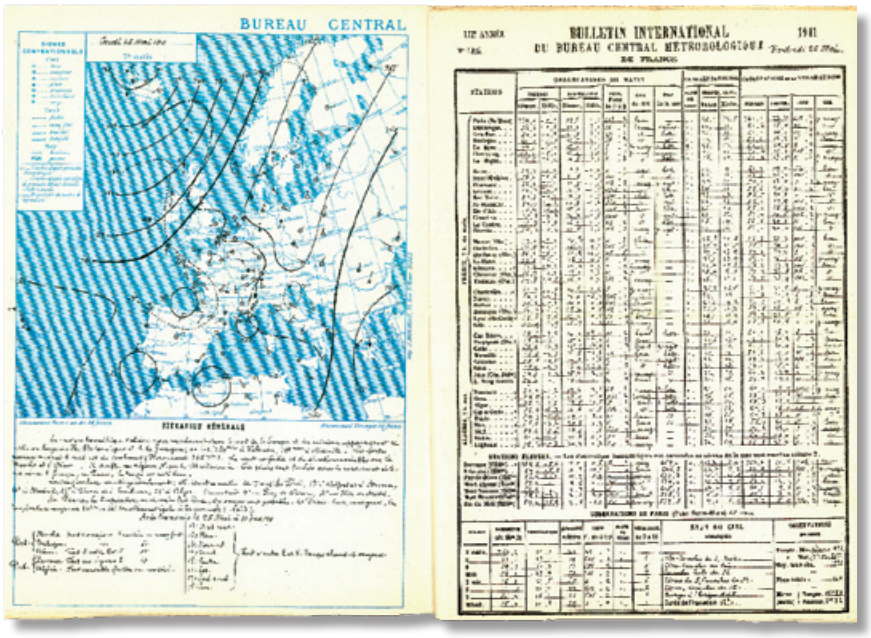

Analysis and observations from May 1911. Reproduction of two pages from Vol. 121 of the '*Bulletin International du Bureau Central Météorologique de France*', showing a hand-drawn weather analysis for 25 May 1911 together with station observations made on the following day.

very labour-intensive and therefore quite expensive. An exciting and potentially groundbreaking development in this area involves the use of the Internet to engage the public at large. Two new websites have launched recently that present images of historic hand-written weather logs and allow a user to key in data values using a simple interactive form. The result is then used to populate a database with digital records. Quality control of the data is achieved by matching multiple digitisations of each image obtained from different users.

Clearly this approach to digitisation of climate records can only succeed if a very large number of users participate. A previous crowd-sourcing project aimed at the classification of millions of images of galaxies – ◆ http://www.galaxyzoo.org has generated an overwhelming response. Perhaps the general public will be even more enthusiastic about helping to improve our understanding of the Earth's climate.

Co-operation Agreement with Israel signed

MANFRED KLÖPPEL

On 28 October 2010, Mr Israel Katz, Israeli Minister of Transport and Road Safety, and Mr Dominique Marbouty, Director-General of ECMWF, signed a co-operation agreement at ECMWF's headquarters. Dr Henia Berkovich, Director of the Israeli Meteorological Service, attended the ceremony. The agreement entered into force on the date of signature. Israel is ECMWF's fifteenth Co-operating State.

Co-operation agreements offer full access to ECMWF real-time products, archive data and software tools, as well as access to ECMWF training facilities.

Minister Katz stated: "I take great pleasure in signing this co-operation agreement with the European Centre for Medium-Range Weather Forecasts, the world leader in numerical weather prediction. It is very important for Israel to have this close link to this centre of excellence. The information we will receive from ECMWF will be a great help to Israeli institutions to deliver top quality services to the Israeli people. I am confident that in particular the Israeli Meteorological Service will benefit immensely from this close co-operation. We very much value this agreement and the benefits it will bring to the people of Israel."

Dr Berkovich said: "This co-operation agreement is highly significant for the Israeli Meteorological Service. I am sure that closer collaboration with ECMWF will enable us to issue earlier advice on the likelihood of extreme weather, such as heat waves we experienced in the past years. We will be able to pass on the information we receive as a Co-operating State to both the public and the authorities responsible so that they can prepare for and respond to adverse weather events more effectively. We welcome the opportunity to share knowledge and expertise with our colleagues at ECMWF and will use ECMWF's products to improve our forecasts and extend their range."

Co-operation Agreement with Israel. Henia Berkovich, Israel Katz and Dominique Marbouty at the signing of the Co-operation Agreement.

Mr Marbouty said: "ECMWF owes its reputation as world leader in the field of global numerical weather prediction in the medium range to its close collaboration with the meteorological community worldwide. Governments are becoming increasingly aware of the need to improve the quality and accuracy of weather prediction in order to obtain advance warning of severe weather events such as storms, heat waves and floods. I look forward to working closely with the Israeli Meteorological Service and am pleased to offer the agency access to all our products, especially medium-range and seasonal weather forecasts."

To date, Co-operation Agreements have been signed with:

- Bulgaria
- Croatia
- Czech Republic
- Estonia
- Iceland
- Israel
- Hungary
- Latvia
- Lithuania
- Montenegro
- Morocco
- Romania
- Serbia
- Slovakia
- Slovenia

Outstanding Editor Award for Florian Pappenberger

ERLAND KÄLLÉN

Florian Pappenberger, a member of ECMWF's Predictability and Diagnostics Section, has received the Outstanding Editor Award from the European Geosciences Union (EGU). The award is in recognition of his excellent services as editor of '*Hydrology and Earth System Sciences*' (HESS) in 2009.

HESS is an international open access journal for the publication of hydrological research placed within a holistic Earth System Science context. It has the highest impact factors of all hydrological journals.

HESS encourages fundamental and applied research that seeks to understand the interactions between water, weather, earth, ecosystems and man. It has the ambition to serve not only the community of hydrologists, but all earth and life scientists.

The journal explicitly encourages submissions in the area of hydro-meteorology. For further information see:

- http://www.hydrology-and-earth-system-sciences.net

ECMWF workshops and scientific meetings in 2011

BOB RIDDAWAY

Forecast Products Users' Meeting (8 to 10 June 2011)

ECMWF organizes annually a meeting of users of its medium-range and extended-range products. The purpose of the meetings is to:

- Give forecasters the opportunity to discuss their experience with and to exchange views on the use of the medium-range and extended-range products, including the ensemble.
- Review the development of the operational system and to discuss future developments including forecast products.

User registration from Member States and Co-operating States should be communicated via the National Meteorological Service of that country. Invitations will be mailed to the Member States early in 2011.

- http://www.ecmwf.int/newsevents/meetings/forecast_products_user/

ECMWF/WGNE/THORPEX Workshop on 'Treatment of model error in forecast models and data assimilation' (21 to 24 June 2011)

Model error plays a major role in weather and climate prediction uncertainty. Recently it has become clear that model error also plays a role in analysis uncertainty. This workshop will focus on the different approaches to the representation of model error over a range of forecast timescales, from multi-model ensembles, to perturbed parameters and stochastic parametrization. Methods to verify and even combine these different representations of model uncertainty will be discussed.

This extended workshop is co-sponsored by WGNE and THORPEX-PDP Working Group. Workshop attendance is by invitation only.

- http://www.ecmwf.int/newsevents/meetings/workshops/2011/THORPEX/

ECMWF 2011 Annual Seminar on 'Data assimilation for atmosphere and ocean' (5 to 8 September 2011)

Variational data assimilation has been successfully developed and used operationally at ECMWF; today the variational system is a pre-requisite for the assimilation of satellite data and effective use of conventional observations in the atmosphere. Ocean data assimilation is also an integral part of the monthly and seasonal forecast systems.

An extension of variational techniques including longer assimilation

windows and weak constraint methods, to allow for inclusion of model error estimates, are current research areas. Also ensemble based assimilation systems are currently under development and combined with the variational technique to allow for a flow-dependent estimation of background error variances and covariances.

The Ensemble Kalman Filter method has been applied to operational NWP and Extended Kalman Filter methods have been developed for surface parameter assimilation. The development of ensemble-based assimilation techniques implies that initial state perturbation methods and the representation of model error are essential elements of data assimilation systems thus providing close links with ensemble prediction methods.

The seminar will give a pedagogical review of the principles behind data assimilation techniques and provide detailed descriptions of the currently used assimilation techniques. In addition consideration will be given to:

- Observation data sources and their intrinsic properties will be given.
- Future developments in data assimilation such as ensemble based methods and weak constraint variational methods.
- Challenges related to the design of efficient data assimilation schemes on future computer architectures will be addressed.

A registration form and further information will be available from:

- http://www.ecmwf.int/newsevents/meetings/annual_seminar/2011/

ECMWF/GABLS Workshop on 'Diurnal cycles and the stable atmospheric boundary layer' (week of 7 to 11 November 2011)

The diurnal cycles of temperature and wind are strongly influenced by small-scale atmospheric processes in the stable boundary layer, in particular due to turbulent diffusion, gravity waves and radiation. Also the thermal coupling with the underlying soil through vegetation and snow plays an important role. Most large-scale atmospheric models utilize rather diffusive boundary layer schemes resulting in stable boundary layers that are too thick and which show too little wind turning. Furthermore, the small-scale stable boundary layer processes have strong implications for winter-time temperature over continental areas, and as such making the topic an important climate issue as well. Night-time wind extremes above the boundary layer are often not well represented and highly relevant for wind energy. However, attempts to implement less diffusive boundary layer schemes have shown poor objective scores and difficulties with night-time and winter-time continental temperatures. The workshop will review the relevant research, consider the available schemes, explore the recent data sets and make recommendations for large-scale models.

The workshop is co-sponsored by the GEWEX Atmospheric Boundary Layer Studies Working Group (GABLS). Workshop attendance is by invitation only.

- http://www.ecmwf.int/newsevents/meetings/workshops/2011/GABLS/

13th Workshop on 'Meteorological Operational Systems' (31 October to 4 November 2011)

The objective of the workshop is to review the state-of-the-art of meteorological operational systems and to address future trends in:

- The use and interpretation of medium and extended range forecast guidance.
- Operational data management systems.
- Meteorological visualisation applications.

Further information will be available from:

- http://www.ecmwf.int/newsevents/meetings/workshops/2011/MOS_13

Update on China's FY-3 meteorological satellites

BILL BELL

China's FY-3 series of polar orbiting meteorological satellites has the potential to become an important component of the Global Observing Sytem and provide valuable data for NWP data assimilation systems. The first satellite, FY-3A, was launched in May 2008 and has been evaluated at ECMWF. The second, FY-3B, was successfully launched from China's Taiyuan Launch Centre on 5 November 2010.

As part of a cooperation agreement between the China Meteorological Administration (CMA) and ECMWF a scientist from CMA's National Satellite Meteorological Center (NSMC), Dr Qifeng Lu, visited ECMWF during 2009 to evaluate data from the FY-3A instruments. The findings from his work were described in *ECMWF Newsletter No. 122* (Winter 2009/10). Dr Lu returned to ECMWF during summer 2010 to complete a detailed investigation into the performance of the FY-3A Microwave Temperature Sounder (MWTS). This work revealed several sources of bias in the data, using new techniques, and developed corrections for the data which significantly improved the data quality and impact on the forecasts. The results of these investigations were fed back to the FY-3A instrument teams who were able to improve the pre-launch characterisation of FY-3B. Dr Lu has now established close links with the FY-3 engineering teams, thereby improving communications between NWP end-users and the instrument teams.

FY-3A data has been passively monitored in real time since the implementation of IFS Cy36r4 on 9 November 2010. Some minor quality control issues remain with the FY-3A MWTS data and ECMWF is liaising closely with CMA/NSMC to resolve these. It is planned to actively assimilate FY-3A data in 2011.

Extreme weather events in summer 2010: how did the ECMWF forecasting systems perform?

ANNA GHELLI, ANTONIO GARCIA-MENDEZ, FERNANDO PRATES, MOHAMED DAHOUI

THE WEATHER over Europe and Asia during July and August 2010 has been rather unusual.

During the second half of July and beginning of August, a blocking anticyclone over Russia dominated the weather pattern in Europe. Figure 1 shows the analysed geopotential height at 500 hPa and the winds at 200 hPa averaged for the period 15 July to 10 August. The blocking high is visible in the geopotential height field while the jet meanders around it. At the end of July, it is this jet that drives cold air towards the Indian Ocean which interacts with low-level warm and humid air and initiates the heavy rainfall in Pakistan. During the blocking period the position of the anticyclone favoured a cold northerly airflow that ended the warm spell over Western Europe. At the same time warm air from Africa reached Russia leading to a heat wave with temperatures rising to unprecedented levels.

Both the Russian heat wave and the severe rainfall in Pakistan will be discussed with the focus on the performance of the ECMWF's deterministic forecasts and Ensemble Prediction System (EPS).

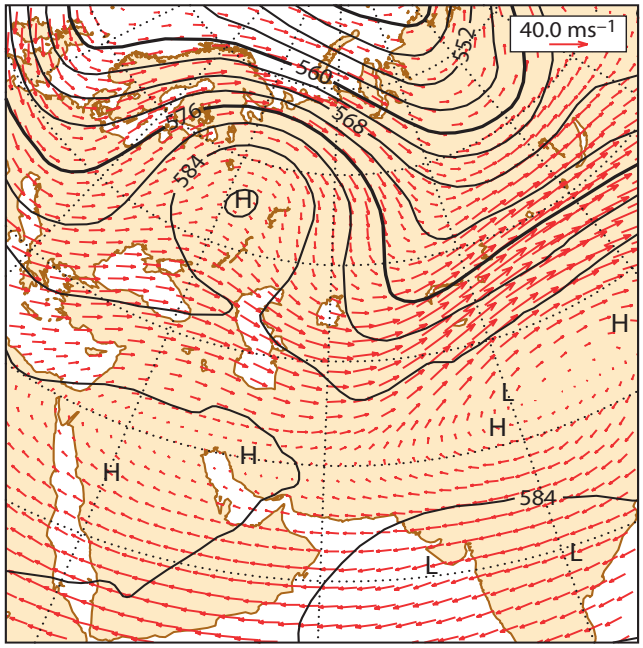

Figure 1 Geopotential height at 500 hPa and wind at 200 hPa averaged over the period 15 July to 10 August 2010.

Russian heat wave

ECMWF's model suites (deterministic and ensemble forecasts) were consistently forecasting the onset and persistence of the blocked pattern both in the medium-range and monthly forecasts. The blocking pattern during the first week in August was forecast four weeks in advance with the monthly forecasting system displaying positive anomalies of geopotential height at 500 hPa over Russia from the forecast run from 8 July 2010. Subsequent forecasts consistently indicated the presence of positive anomalies over Russia which became stronger as the forecast lead-time decreased.

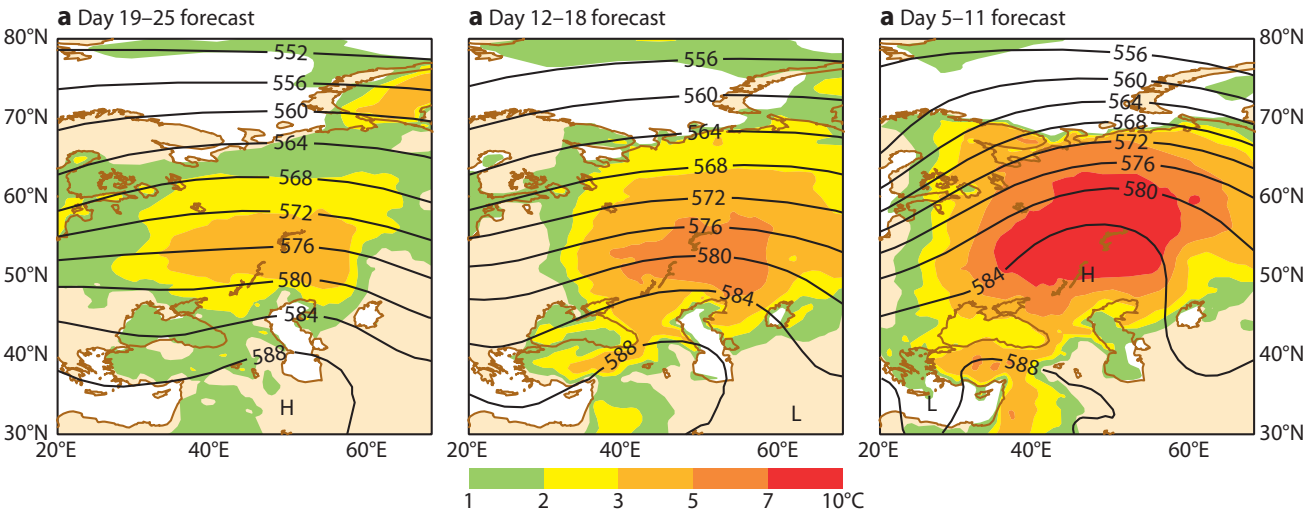

Figure 2 Forecasts of 2-metre temperature weekly anomaly (°C) for the first week in August based on forecasts for (a) days 19 to 25, (b) days 12 to 18 and (c) days 5 to 11. The anomalies are shaded as in the legend and the mean weekly forecast for the geopotential at 500 hPa is contoured.

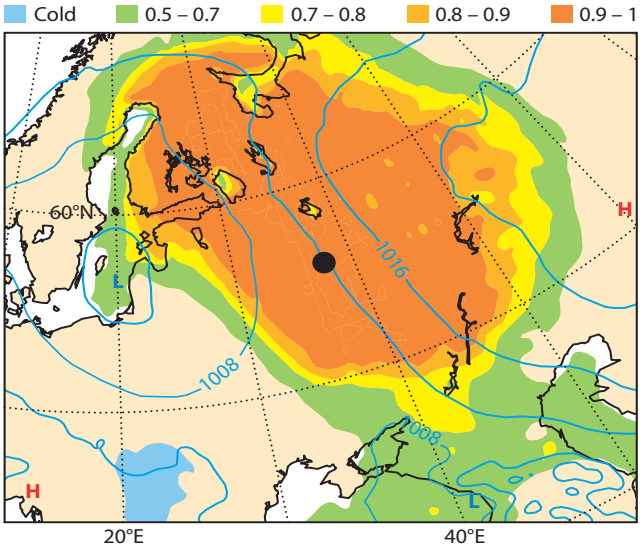

Figure 3 Four-day forecast of EFI values from 00 UTC on 25 July 2010 for the Russian heat wave. The black dot indicates the location of Moscow.

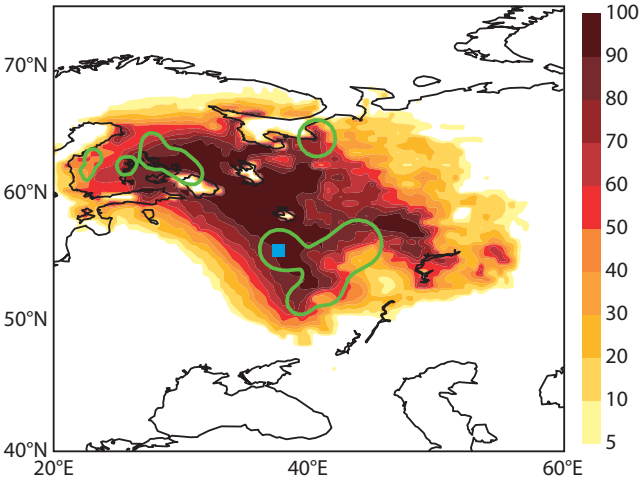

Figure 5 90-hour probability forecast (%) of the 20-year extreme temperature for the forecast started at 00 UTC on 26 July and valid for 18 UTC on 29 July 2010. The areas bounded by green lines represent the 'radius of influence' for the SYNOP stations reporting a 20-year return period to highlight observed events at each station. Moscow is marked by a blue square. Return values are obtained from the European Climate Assessment & Dataset Project.

Figure 2 illustrates the forecasts of 2-metre temperature weekly anomalies in Russia and the weekly mean for the geopotential at 500 hPa. Three weeks before the event the anomalies of 2-metre temperature from the monthly forecast (Figure 2a) indicated unusually warm conditions during the first week of August, with this signal being consistent in subsequent forecasts (Figures 2b and 2c). A verification of the heat wave anomalies indicates that the forecast anomalies were only slightly less pronounced than those analysed.

The highest observed temperatures occurred during the last week of July and the first week of August when temperatures soared to record values of up to 39°C at Moscow Domodedovo airport and Moscow Observatory. The ECMWF EPS forecast the heat wave on 29 July as illustrated by the four-day forecast of the extreme forecast index (EFI) shown in Figure 3. This shows an extensive area with high values from the Ural Mountains to the western border of Russia. The EFI for Moscow (black dot in Figure 3) is close to 1 (corresponding to the highest probability of temperatures above the climate values) and a significant risk of extremely hot weather is also forecast for southern Finland.

The shorter-range EPS forecast also indicated maximum temperatures well above climate values (the climate used refers to an 18-year model climate) for an extended period as shown in the 15-day EPSgram for a location close to Moscow (Figure 4). Indeed the EPSgram shows maximum temperatures exceeding the 99th percentile of the climate by 4° to 5°C, i.e. a very extreme event.

The rarity of extreme weather events can be expressed in terms of their return period; rarer events have longer return periods which can be assessed statistically from their frequency of occurrence in long time series. Figure 5 shows the EPS probability (at day 4) of exceeding the temperature extreme at each location that statistically would be expected to occur on average once in any 20-year period, i.e. the temperature with a 20-year return period. During the Russian heat wave, the EPS predicted 20-year extreme temperatures with very high probability on 29 July. To generate this probability forecast in terms of return period, the following steps are performed.

- The daily maximum temperature values are extracted from the 18-year EPS model climate at each grid point and used to fit a statistical frequency distribution function appropriate for the analysis of extremes (*Coles*, 2001).
- At each location, the temperature value associated with

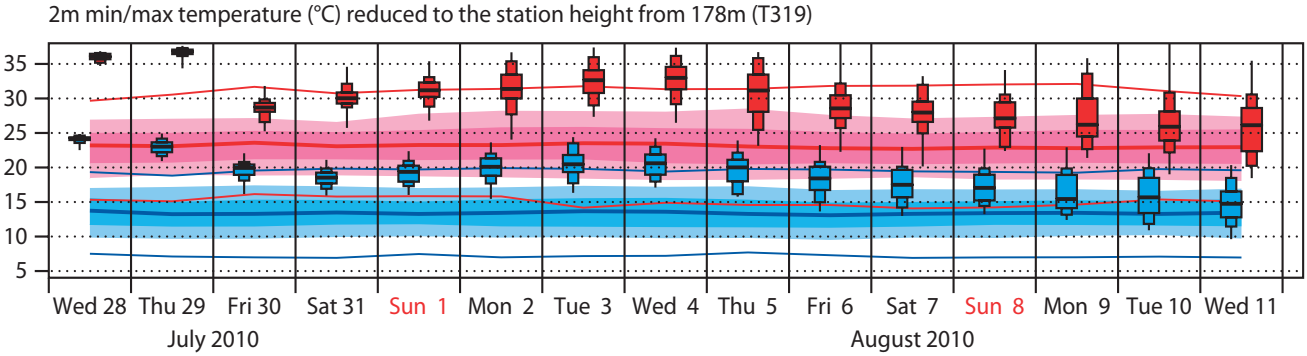

Figure 4 Extract from the 15-day EPSgram for a location near Moscow (55.88°N, 37.50°E). The maximum of temperature (Tmax) and its climate distribution are shown in red. The shaded area is the climate and the lines represent the 1st and 99th percentile. The minimum temperature and its climate distribution are also included (blue).

any given return period (e.g. 20 years) is obtained from those distributions.

- The forecast probability of exceeding the n-year extreme temperature is computed at each location as the number of EPS members with the event divided by the size of the ensemble (i.e. 51 for the current EPS).

In Figure 5 probabilities higher than 80% can be seen in eastern Finland and northern Russia where the 20-year extreme temperature was indeed exceeded in several places as shown by the contoured areas. In some locations the EPS even indicated a high probability of exceeding the 75-year extreme temperature, thereby conveying a high level of confidence for the very unusual temperatures four days in advance.

As the heat wave relentlessly influenced the life of millions of Russians, correctly forecasting the end of the blocking became of crucial importance, as a breaking of the anticyclonic conditions implied cooler air being allowed in over Russia. Figure 6 shows the Hovmöller plot of a 20-day analysis followed by a 10-day forecast from 12 UTC on 18 August 2010. It indicates the time evolution (on the ordinate) of geopotential anomaly at 500 hPa averaged over a range of latitudes (35°N to 60°N) versus the longitude. The red area (positive anomaly) centred at 50°E indicates the analysed stationary blocking pattern. On the 18th, the short-range forecast correctly shows the breaking of the blocking with

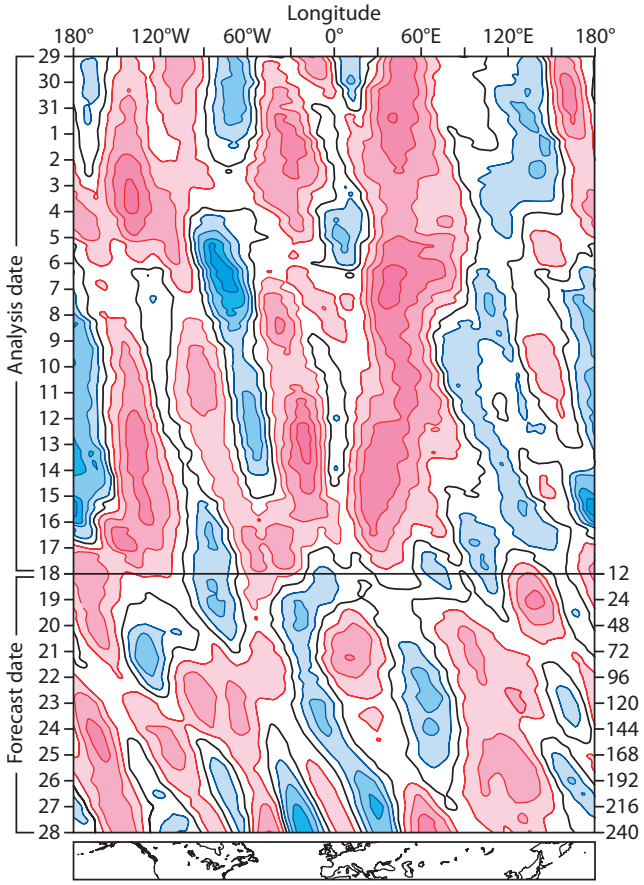

Figure 6 Hovmöller plot of geopotential anomaly showing the 500 hPa geopotential anomaly averaged over 35°–60°N for the analysis from 12 UTC on 29 July to 12 UTC on 18 August followed by the forecast from 12 UTC on 18 August 2010.

a August 2009

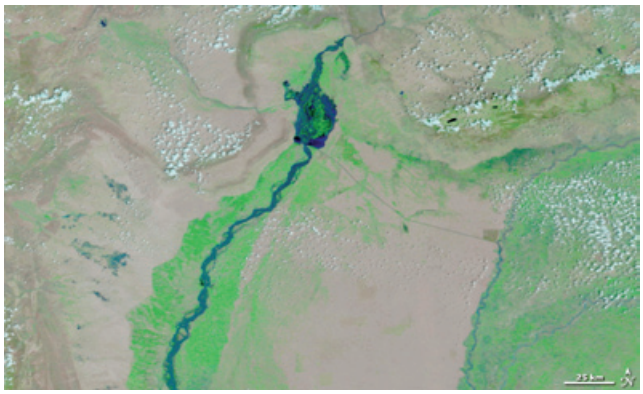

b August 2010

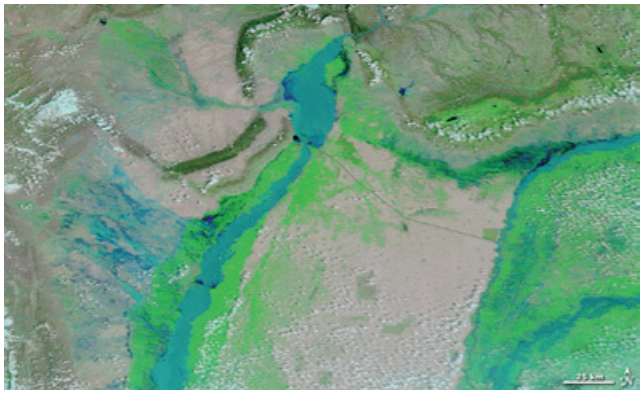

Figure 7 Satellite images of the catchment of the river Indus for (a) August 2009 and (b) August 2010.

negative anomalies moving into Russia as the forecast range progresses (blue area, backward tilted). Indeed, indications of the end of the blocked flow were evident in the deterministic high-resolution forecast run from 12 August 2010; that is the end of the blocking was forecast with a 6-day lead-time.

The 6-day EPS forecast based on 12 August 2010 indicated a circulation change. The spread of the ensemble associated with this circulation change was small suggesting a forecast with a high degree of confidence. Moreover, the monthly forecasts showed the weakening of the warm anomaly over Russia in the period 16–22 August, 3 weeks in advance.

Rainfall in Pakistan

The devastating floods that hit Pakistan at the end of July cannot simply be ascribed to a particularly active Indian Monsoon. This is illustrated by the amount of precipitation received in a single day which exceeded half of the annual rainfall (see *'Extreme weather in August 2010'* by Julia Slingo available from:

www.metoffice.gov.uk/corporate/pressoffice/toolkits.html)

The rather unusual weather pattern during the last week of July, with cold air at higher levels and warm and humid air at low levels, triggered excessive amounts of rain which caused severe flooding along the river Indus. Comparing the satellite images of Pakistan in August 2009 (Figure 7a) and in August 2010 (Figure 7b) gives an indication of the severity of the flooding.

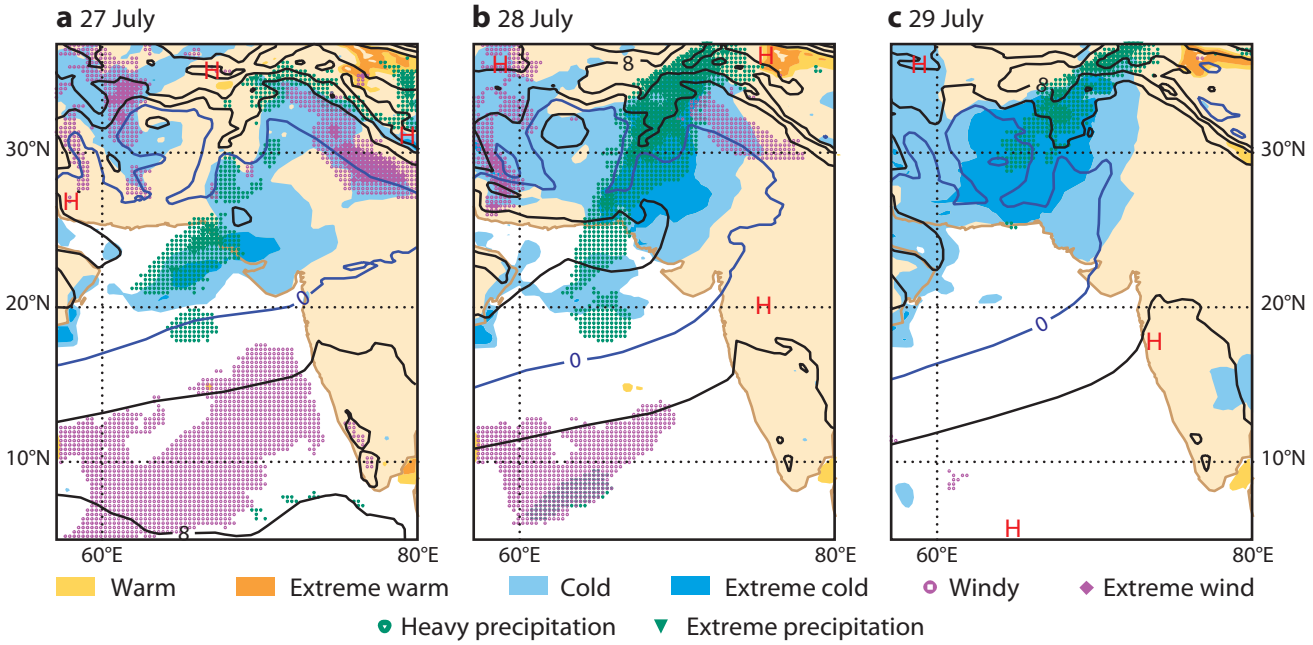

Figure 8 EFI categories for Pakistan and neighbouring India for three consecutive days: (a) 27 July, (b) 28 July and (c) 29 July 2010. Green dots/triangles: heavy/extreme precipitation; Light/dark blue shading: anomalous cold temperatures; Magenta dots/diamonds: windy/extreme wind.

The ECMWF high-resolution deterministic forecast indicated with great consistency the influx of warm and humid air from the ocean 5 days ahead of the event, with accumulated precipitations over 4 days of 400 mm along the river Indus; this is in good agreement with the reported rainfall amounts.

The EFI had a clear signal with values close to 1 (maximum risk) for precipitation well above climate values. A sequence of three plots showing the EFI values for Pakistan and neighbouring parts of India depicts the build up of the heavy precipitation event from 27 to 29 July (Figure 8).

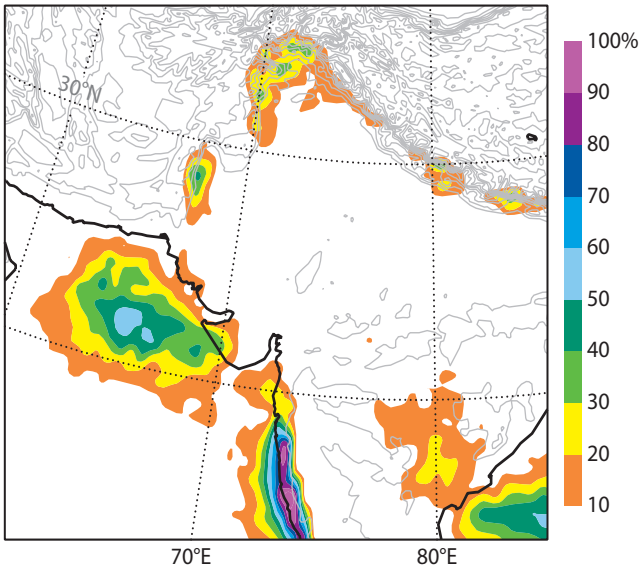

Figure 9 Day-9 probability of rainfall exceeding 100 mm over four days (accumulated from day 5) for Pakistan based on the forecast from 00 UTC on 22 July 2010 along with the contours of the orography.

Figure 9 shows the probability of exceeding 100 mm over a period of 4 days. The shaded areas correspond to different probability thresholds while the contours serve as indicators of the orography. The regions of high probability located over the Indian Ocean and the western side of the Indian peninsula correspond to areas affected by the monsoon which is active during the summer season (May through to September). Areas of large probability of exceedance are also located in the mountainous areas (Hindu Kush and Karakoram ranges) of Pakistan and India and along the river Indus where the probability was already up to 40% nine days before the event. Subsequent forecasts (shorter range) see this probability of exceedance increase to 50%.

The monthly forecast predicted exceptional rainfall over Pakistan (during the last week in July) well in advance. Four weeks before the event the predicted weekly anomaly was between 30 to 80 mm depending on the area. These values compare well with the analysed precipitation (the short-range forecast is hereafter used as a proxy for the observed amounts) for the period. Figure 10a shows the precipitation analysis for the last week in July and the four forecasts verifying on the analysis are given at Figures 10b, 10c, 10d and 10e.

Forecasting extreme weather events

The extreme weather events in summer 2010 were well predicted by ECMWF forecasting systems. The monthly forecasting system gave a good indication of the temperature anomaly over Russia three weeks in advance and high temperatures were consistently forecast in the medium range. Indeed the EFI gave a good indication of the risk four days ahead and the return period signalled the severity of the event. It is noteworthy that the crucial identification of the breaking of the blocking was also forecast with a high level of confidence by the EPS with a six-day lead-time.

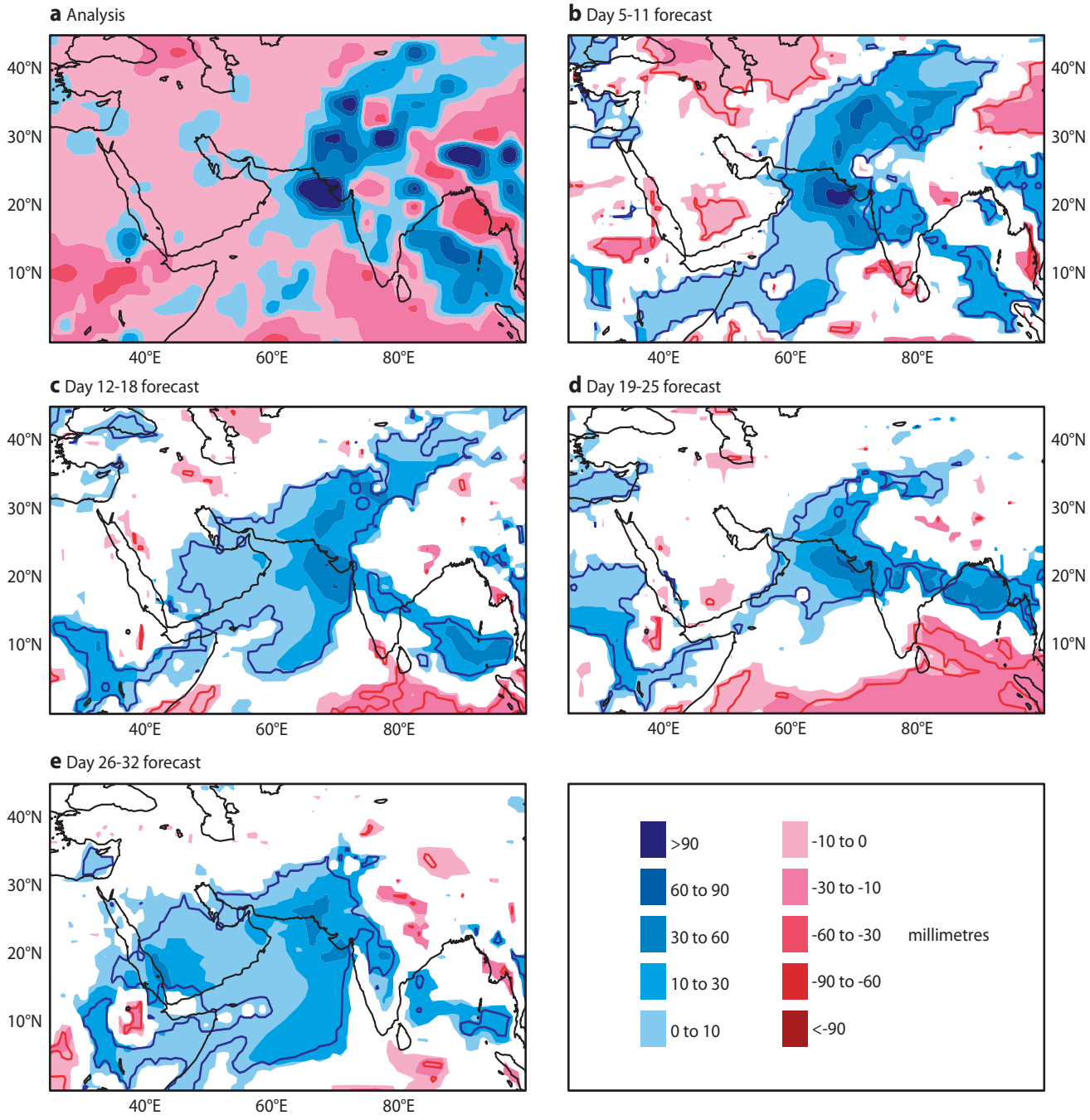

Figure 10 (a) Analysed precipitation anomaly (mm) for the last week in July (the 24-hour forecast has been used as proxy for the analysed values) and the corresponding forecasts for (b) days 5 to 11, (c) days 12 to 18, (d) days 19 to 25, and (e) days 26 to 32 that all verify with the analysed field. The shaded areas are significant at the 10% level.

Both the EPS and deterministic models forecast the heavy precipitation in Pakistan with a high level of accuracy, at least in terms of spatial distribution and timing. The exceptional nature of the situation was signalled by the EFI five days before the event. However, a more extensive evaluation of the performance is more difficult because of the lack of observations in the area

The early warning of severe weather events is one of the key goals of ECMWF and in these severe events the ECMWF EPS and deterministic model gave useful guidance at least five days in advance. The monthly forecasts were also very successful and demonstrated the added value they can offer to the medium-range forecasts.

ECMWF strives to offer quality forecasts in the medium and longer time scales. Regular increases in horizontal and vertical resolutions as well as improved data assimilation and representation of physical processes are such that this quality can be achieved and pushed to higher levels. In addition, further developments in providing a better representation of model and initial condition uncertainties will undoubtedly provide more accurate probability forecasts.

FURTHER READING

Coles, S., 2001: *An Introduction to Statistical Modelling of Extreme Values.* Springer-Verlag

Weak constraint 4D-Var

YANNICK TRÉMOLET, MIKE FISHER

THE FUNDAMENTAL purpose of 4D-Var (as implemented by ECMWF in 1997) is to correct a short-range forecast based on observations available since the last assimilation time. In this system, the correction is calculated in a four-dimensional domain: the three spatial dimensions and the time dimension. The atmospheric state over this domain is entirely determined by the state at the beginning of the assimilation window through the use of the forecast model. So, although 4D-Var finds the solution over a four-dimensional domain, it does so by adjusting the three-dimensional initial condition of the forecast (known as the control variable). This is equivalent to making the assumption that the forecast model is perfect over the length of the assimilation window. The model is said to be imposed as a strong constraint in the 4D-Var optimization problem.

Since 4D-Var became operational in 1997, many aspects of the data assimilation system have improved, and the amplitudes of many types of errors have reduced. The assumption that the model is perfect, or that model error is small enough relative to other errors in the system to be ignored, has become questionable. This is compounded by the fact that longer assimilation windows are desirable. Over long ranges, model error becomes larger and should be accounted for in the data assimilation process.

Relaxation of the perfect model assumption requires a modification of the 4D-Var algorithm. The resulting method is known as weak constraint 4D-Var. The remainder of this article will describe how weak constraint 4D-Var has been implemented in cycle 35r3 (8 September 2009) of ECMWF's Integrated Forecasting System (IFS). Also, directions for future research will be outlined.

Accounting for an imperfect model

The data assimilation process is a statistical problem where the best estimate of the state of the atmosphere is sought, given knowledge about the state and the error characteristics of the various sources of information. In weak constraint 4D-Var, the model is considered in the same way as the other sources of information, including taking into account that there is a degree of uncertainty about the information from the model.

There are several practical approaches to account for model imperfection in 4D-Var and to estimate model error (*Trémolet*, 2006). The first approach that has been implemented at ECMWF comprises adding a forcing term to the model which in principle would compensate for model error within each time step. The 4D-Var control variable is then augmented by these forcing terms and a term is added to the cost function to penalize model error according to its statistical characteristics. 4D-Var then determines what the optimal forcing terms should be, given the prescribed model error statistics and all other available information.

The forcing term at each time-step has in principle the same number of components as the model state. Thus the size of the control variable is multiplied by the number of time steps compared to the strong constraint 4D-Var control variable. This is unaffordable from a computing point of view but, even more importantly, there is not enough information available to determine so many parameters or to estimate their error characteristics, such as space and time correlations or flow dependence. Some simplifications are necessary to solve the weak constraint 4D-Var problem.

In our initial implementation of weak constraint 4D-Var, the main simplification is to assume that model error is constant in time over the length of one assimilation 'window' (currently 12 hours at ECMWF). With this assumption, the size of the control variable is doubled with respect to strong constraint 4D-Var, which is manageable on today's supercomputers. The model error covariance matrix becomes a three-dimensional matrix of the same dimension as the background error covariance matrix.

Model error statistics

Covariance statistics for both background and model errors are generated from large sets of samples. In both cases, since we do not know the true state of the atmosphere, we cannot explicitly generate the required samples of errors, and must instead turn to proxy quantities whose error statistics are similar to those of the actual errors. In the case of background errors, the proxy errors are generated as differences between forecasts from an ensemble of data assimilations. However, it is far from clear how to generate proxies for model error. In the current implementation of weak constraint 4D-Var, we use samples of differences between model tendencies from an ensemble of forecasts. The idea is that if each state from an ensemble is a possible representation of the actual atmospheric state, then the differences between the various tendencies generated by the model for different ensemble members give an indication of the likely size of the model uncertainty (see *Trémolet*, 2007 for more details).

The model error covariance matrix uses a spectral representation, as previously used for the background error. Since the covariances are computed from instantaneous quantities, rather than from short-forecast integrations, the correlation length scales for all variables are shorter in both the horizontal and the vertical. In this implementation, the covariances in one variable (temperature, say) are assumed to be uncorrelated with errors in other variables (e.g. vorticity). In reality, the errors affecting the model variables are not independent.

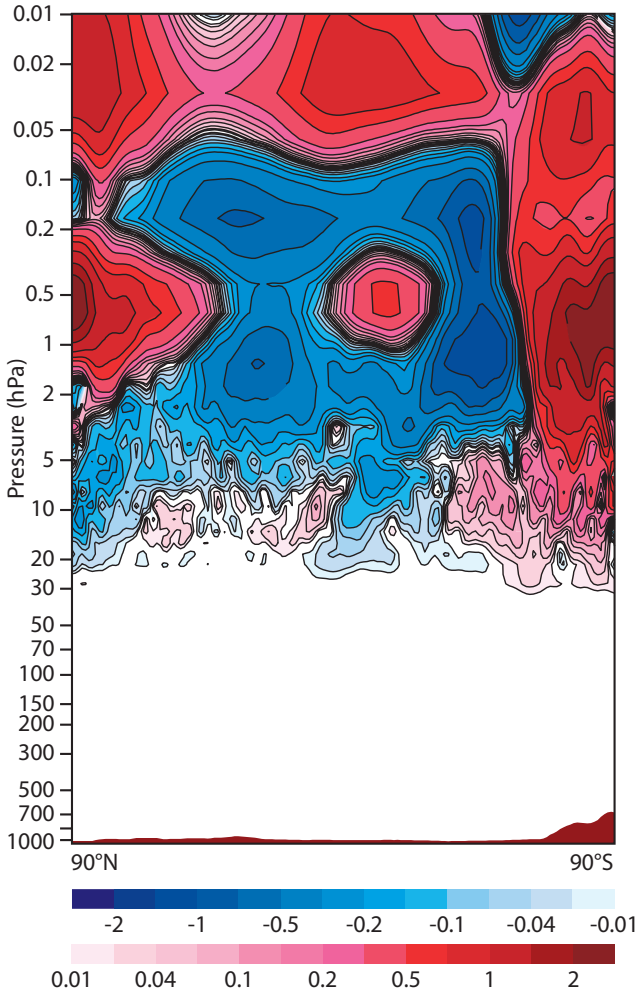

Figure 1 Monthly-mean temperature model error forcing (K/12h) in the stratosphere estimated by weak constraint 4D-Var for July 2008 (IFS Cy35r2, T255).

So far attempts at accounting for multivariate relationships in model error have not been successful but this is an area for further research in the future.

More generally, very little is known about model error or its statistics. Whereas the estimation and modelling of the background error statistics has been an active area of research for many years, very little research has taken place to estimate or represent model error statistics in data assimilation. Moreover, the model error covariance matrix is an order of magnitude more complex than the background error covariance matrix due to the additional time dimension it involves.

Despite the relative lack of research into model error, a few approaches can already be identified. For example, ECMWF's Ensemble Prediction System (EPS) includes stochastic terms to represent model error. Such terms are mostly designed to make the ensemble prediction spread match the forecast error at medium range. Data assimilation is primarily a short-range problem. Nevertheless, valuable information and experience could be extracted from developments with the EPS. A practical step towards using the schemes developed in the EPS could be achieved by recognising that the method used by the stochastic backscatter scheme to convert the white noise output of the random number generator into a representation of spatially and temporally correlated model error, can be considered as defining the square-root of the model error covariance matrix. Use of this approach would allow a representation of model error in 4D-Var that is consistent with the approach adopted in the EPS.

In practice, observations are the only independent source of information available to estimate the actual model error. Ideally, estimations of model error statistics should use this information. Two directions of research can already be considered.

- Explore observation space consistency diagnostics, such as the ones proposed by *Desroziers et al.* (2005). Since strong constraint 4D-Var does not account for model error, any imperfect model should introduce inconsistencies with respect to the assumptions being made. The difficulty is then to extract useful model error information out of the internal signs of inconsistency.
- Extend work carried out in the context of lagged Kalman smoothers. It has been shown in that context that the difference in fit to the observations for analysis windows of different lengths can be attributed to model error. Again, the difficulty is to extract useful model error information from this signal.

Model error statistics are important for all data assimilation methods, including ensemble Kalman filters (where it is currently treated in a very crude way). Yet, model error is one of the least understood quantities in data assimilation. This is surprising, given the importance of the model in the process. Better estimation of model error statistics will be a major topic of research in data assimilation in the coming years.

Systematic model error

In the first implementation of weak constraint 4D-Var, model error is assumed to be independent from one assimilation cycle to the next. Although there are systematic errors that vary on longer timescales (seasonal for example), this is a safe approach that prevents positive feedback effects between model error on one hand and initial condition or observation bias correction on the other hand.

Experimentation is currently underway to account for model error on the longer timescales, such as temperature biases in the stratosphere in polar regions which typically vary on a seasonal timescale. This type of error is the largest in amplitude and can seriously affect the assimilation of high peaking channels for many satellite radiance observations. Since these biases vary on timescales that are slower than the length of the assimilation cycle, it is important to retain information from one cycle to the next. This is achieved by re-writing the model error penalty term in the 4D-Var cost function as a term that penalizes the variation in model error from one cycle to the next rather than the total model error. With this setup, however, there is no constraint to prevent model error from growing progressively over a large number of assimilation cycles. This could potentially have a major impact on the assimilation system.

Impact of the weak constraint 4D-Var

Weak constraint 4D-Var corrects model errors by adding a forcing term to each of the model's prognostic equations, in order to make the model consistent with the available observations. As it is known that errors in the ECMWF system are on average larger in the stratosphere than at lower levels, we have taken a cautious approach and initially restricted the model error term to apply only above 10 hPa (with a transition zone down to 40 hPa).

Figure 1 shows the monthly-mean model error forcing for temperature for July 2008. This indicates that to match the observations in the stratosphere and mesosphere there is the need for a systematic warming at polar latitudes and near the top of the model, with cooling at mid-latitudes in the upper stratosphere and mesosphere. Figure 2 shows the associated mean temperature analysis increments for strong and weak constraint 4D-Var. Note that the mean analysis increment is significantly reduced in weak constraint 4D-Var, which has correctly identified that the need for systematic corrections is due to errors in the model. Although the difference is relatively modest, Figure 2 also shows that oscillations in the increments over the North Pole have been removed and that they are reduced in amplitude over the South Pole. These oscillations are believed to be caused by model errors and their reduction should facilitate assimilation of satellite observations sensitive to temperature at these levels. All the results presented here were obtained with IFS cycle 35r2 at the resolution of T255 with 91 levels.

Figure 3a shows the average analysis and first-guess departures for radiances from AMSU-A channel 13 and the mean temperature analysis increment using weak constraint 4D-Var. Also shown is the model error forcing at the model level where this data is the most sensitive. The corresponding information when the model error is cycled and allowed to grow over time is shown in Figure 3b. In this case, the average observation first-guess departure is centred around the zero line which is not so when there is no cycling (red curves). This shows that the short-term forecast is improved by the model error cycling and model error information is retained and useful from one cycle to the next. The seasonal variation in observation bias correction (black curves) is also slightly reduced which goes in the right direction since this variation is due to seasonal variations in the model and not in the observations. The mean analysis increment (green curves) is also closer to the zero line where it should be in an unbiased system. (Note that it is not fully centred around the zero line. Most likely this is due to the fact that AMSU-A

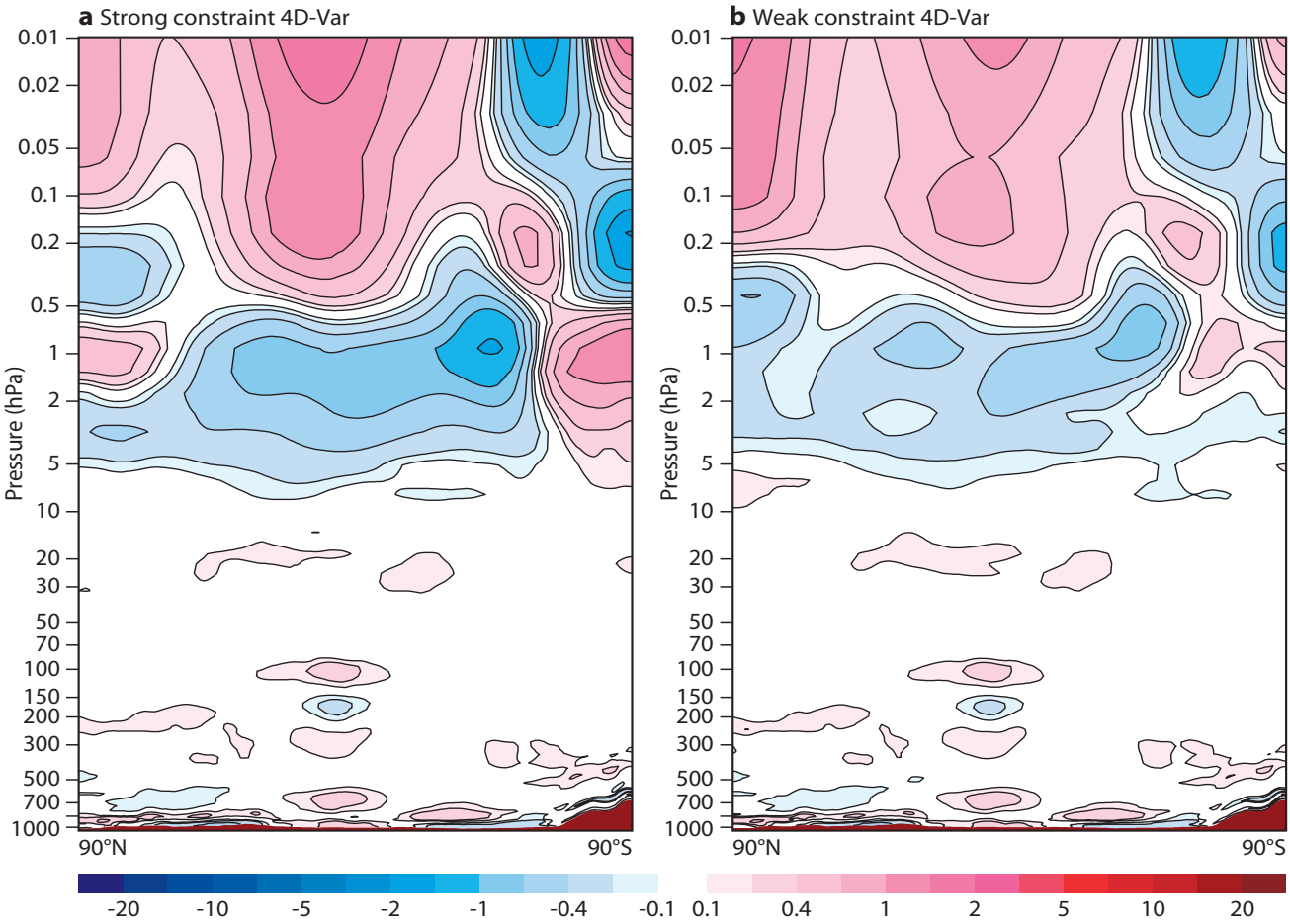

Figure 2 Monthly-mean temperature analysis increments (K) for July 2008 in (a) strong constraint 4D-Var and (b) weak constraint 4D-Var with model error applied in the stratosphere.

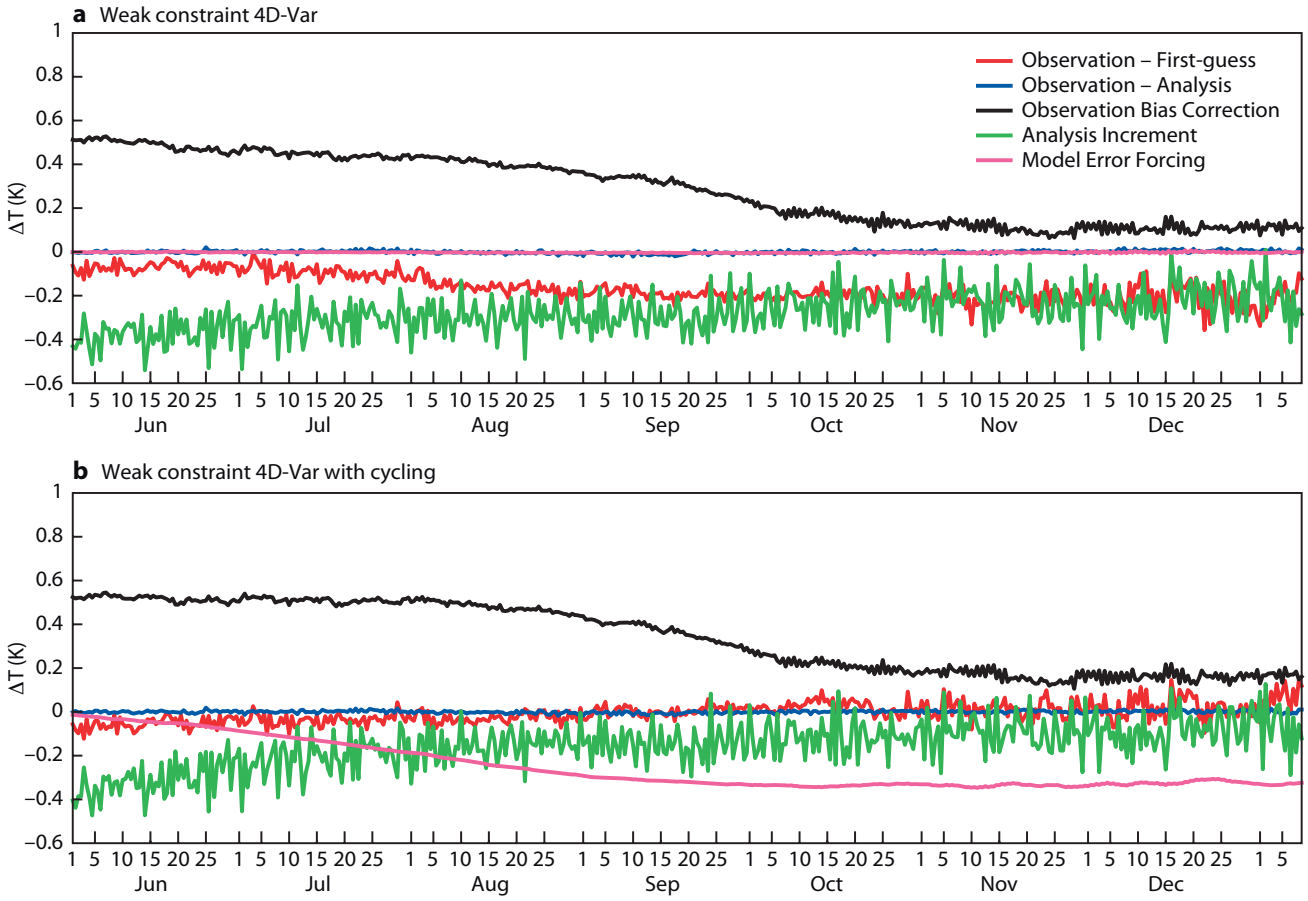

Figure 3 (a) Average analysis and first-guess departure of radiances from AMSU-A channel 13 for July 2008 for the northern hemisphere using weak constraint 4D-Var. Also shown is the mean temperature analysis increment and model error forcing at model level 14 where this channel is the most sensitive. (b) As (a) but the model error is cycled. See text for more details.

channel 14, which also has some sensitivity at that level, is not bias corrected.)

These results give an example of the complex interactions between the model error, the initial condition increment and the observation bias correction in 4D-Var. Overall, model error as estimated in these experiments varies on a slow timescale (the order of a few months on Figure 3) and should probably also vary on shorter timescales. However, interactions with the other parts of the control variable must be examined carefully.

4D-Var uses the covariance matrices of background, observation and model errors to partition the analysis error between the various terms of the cost function. Incorrect specification of any one of these covariance matrices can result in one source of error being misinterpreted as another type of error (e.g. observation error may be misinterpreted as model error). This highlights the necessity for a proper estimation of all the covariance matrices. The large number of available degrees of freedom in the model error makes it particularly important to correctly specify the model error covariances so as to avoid absorbing all the information contained in the observations into the wrong component.

Towards a longer assimilation window

Fisher et al. (2005) have shown that weak constraint 4D-Var with a long assimilation window is equivalent to a full rank Kalman smoother. This can be seen as theoretical justification for a move towards longer assimilation windows in 4D-Var. On a more pragmatic level, it seems obvious that a simultaneous analysis of all relevant observations ought to lead to a better analysis than an artificial splitting of observations into batches of length 12 hours, to be analysed independently. The practical implementation of this idea, however, requires that 4D-Var take into account the variation of model error within the assimilation window. For analysis windows longer than 12 hours, it is no longer sufficient to assume that model error remains constant throughout the window.

Because of the limitations imposed by the incremental 4D-Var algorithm, a long analysis window cannot be achieved with a formulation involving a model error forcing term. (The different-resolution models used in the inner and outer loops of 4D-Var react very differently to the forcing, and diverge significantly over the analysis window, preventing the convergence of the incremental algorithm.) Consequently, the weak constraint 4D-Var cost function has to be formulated directly as a function of the four-dimensional state over the length of the assimilation window. (In practice, for computational reasons, and because of the limited amount of available information, the state variable at regular sub-intervals over the assimilation window would be used.) For each time when the

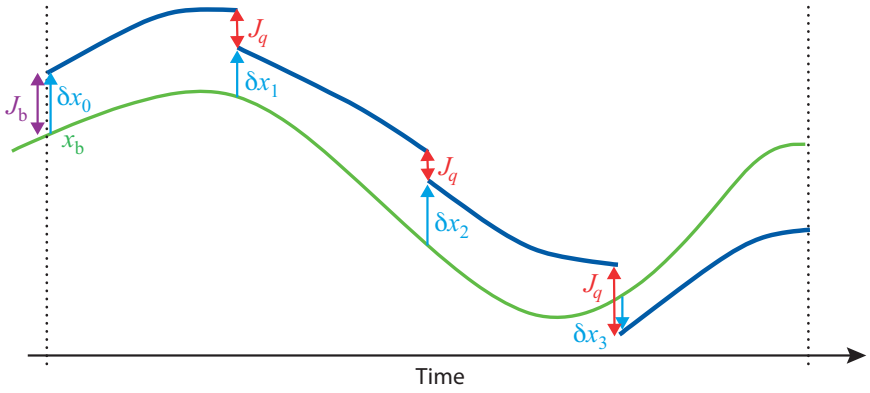

Figure 4 Long window 4D-Var. The schematic diagram shows a single analysis window. The green line represents a model integration started from the background state, which serves as the first guess for the analysis. The control variable for the analysis consists of the departures from the first guess at the start of a set of sub-intervals. Weak constraint 4D-Var adjusts these departures to simultaneously minimise the discrepancy between the analysis and the observations and background state, while also minimising the jumps between the sub-intervals.

state variable is available, a model error term in the cost function is applied to minimize the gap between the state obtained by integrating the model from the previous time when the control variable is defined to the current time. We illustrate this schematically in Figure 4.

This approach has the significant advantage that the state at the start of each sub-interval is known at the start of each iteration of the minimisation. Evaluation of the cost function requires integrations of the model and its adjoint to be performed for each sub-interval, and these model integrations can be performed in parallel. This brings an additional dimension for parallelism in 4D-Var. However, the optimization problem that results from this formulation of 4D-Var has different properties than the (by now well-understood) strong constraint 4D-Var problem. Research into minimisation algorithms and preconditioning methods will be required to develop efficient minimisation strategies.

Further developments

The continued reduction in sources of analysis error since the introduction of 4D-Var means that it is no longer possible to ignore the model itself as a source of error. Accounting for this source of error requires the explicit inclusion of a model error term in the 4D-Var cost function, and a representation of the covariance matrix of model error.

Gathering information about the statistics of model error is difficult, and will be the topic of much future research. Our initial attempts have concentrated on approximating the model error covariance matrix by a covariance matrix of model tendencies. This is unlikely to be an accurate approximation. Nevertheless, it has proved sufficient to allow some significant model errors in the stratosphere to be accounted for in the analysis. Weak constraint 4D-Var was introduced into the ECMWF operational system with the implementation of IFS cycle 35r3 on 8 September 2009.

Improvements to the representation of systematic model error are planned through a modification of the model error penalty term that will allow information about model error to be retained from one analysis cycle to the next.

Although systematic model error is probably the largest component of model error, it will be necessary to account also for the time-varying component. It is likely that this component will have significantly different spatial structure than systematic error, requiring careful construction of the associated error covariance matrix. It is also highly likely that model error is correlated in time, and it will be necessary to take this correlation into account.

We believe that longer assimilation windows have the potential to significantly improve the quality of the 4D-Var analyses. However, to achieve longer windows, we require good statistical models of model error. Longer windows also require changes to the methods used to minimise the cost function. This presents a challenge, requiring the development of new approaches to minimisation and preconditioning. However, it also presents an opportunity to significantly improve the parallel efficiency and scalability of 4D-Var, by allowing parallel model integrations during the evaluations of the cost function. This increase in scalability will be important if 4D-Var is to remain practical on future computer architectures.

FURTHER READING

Desroziers, G., L. Berre, B. Chapnik & P. Poli, 2005: Diagnosis of observation, background and analysis-error statistics in observation space. *Q. J. R. Meteorol. Soc.*, **131**, 3385–3396.

Fisher, M., M. Leutbecher & G. Kelly, 2005: On the equivalence between Kalman smoothing and weak-constraint four-dimensional variational data assimilation. *Q. J. R. Meteorol. Soc.*, **131**, 3235–3246.

Trémolet, Y., 2006: Accounting for an imperfect model in 4D-Var. *Q. J. R. Meteorol. Soc.*, **132**, 2483–2504.

Trémolet, Y., 2007: Model error estimation in 4D-Var. *Q. J. R. Meteorol. Soc.*, **133**, 1267–1280.

Non-hydrostatic modelling at ECMWF

NILS P. WEDI, SYLVIE MALARDEL

HYDROSTATIC EQUILIBRIUM describes an atmospheric state in which the upward directed pressure gradient force (the decrease of pressure with height) is balanced by the (nearly) downward-directed gravitational pull of the Earth. This balance is fundamental to the maintenance of the Earth's atmosphere, and on average the Earth's atmosphere is always very close to hydrostatic equilibrium. This fact has been used to approximate the Euler equations underlying ECMWF's weather prediction model and these approximated 'hydrostatic equations' have been successfully applied at ECMWF for the past 30 years. However, non-hydrostatic effects become important when the horizontal and vertical scales of motion are similar. In atmospheric models this typically arises with horizontal scales of the order of 10 km resolved with grid intervals of order 2 km. For motions of larger scale that are resolved with grid intervals of order 10 km – as in the currently operational model – the hydrostatic approximation is well satisfied.

ECMWF plans to implement a horizontal resolution of 10 km by 2015 for its assimilation and deterministic forecast system, beyond which a non-hydrostatic dynamical core will be required. This article describes the work being carried out to investigate the implementation of a non-hydrostatic dynamical core in ECMWF's Integrated Forecasting System (IFS).

It can be concluded that the non-hydrostatic dynamical core is a possible choice for future, globally uniform high-resolution applications at ECMWF. However, there are issues, in particular with the computational efficiency, that still need to be addressed before it is fit to be used as the dynamical core of the operational model at all resolutions.

Non-hydrostatic formulations

Relaxing the hydrostatic approximation has unfortunately a number of consequences that need to be considered. For example, the unapproximated Euler equations support three classes of waves: acoustic waves, inertia-gravity waves and planetary (Rossby) waves. The hydrostatic approximation conveniently removes vertically propagating acoustic waves, with only insignificant influence on the other two wave types at those scales where the hydrostatic approximation is well satisfied. This leads to the derivation of a time discretisation of the equations that is efficient, stable and accurate even for long time-steps, typically 300 seconds to 1 hour for ECMWF's current NWP applications.

Using the unapproximated Euler equations requires a time discretisation procedure that, despite the presence of fast moving acoustic waves, is equally efficient, accurate and stable. However, a numerical discretisation of the IFS for the unapproximated Euler equations that satisfies all of the above properties for the hydrostatic as well as the non-hydrostatic regime is the subject of ongoing research. Arguably, acoustic waves may be considered irrelevant to numerical weather prediction, which suggests that they could be filtered out a priori (often referred to as anelastic approximation). There is renewed interest in such an approximation, as it may promise an alternative efficient and accurate solution procedure. However, a satisfactory (energy-invariant) form of the governing equations for global-scale applications that eliminates acoustic waves without compromising the other waveforms has yet to be found and is the subject of ongoing research.

Rather than developing a non-hydrostatic dynamical core for the Centre's model from scratch or investigate other existing formulations, it was decided to evaluate the non-hydrostatic formulation developed by the ALADIN group for regional NWP and made available by Météo-France in the global IFS/ARPEGE model framework (*Benard et al.*, 2010). The aim is to assess whether this formulation is able to fulfil the requirements of high accuracy, efficiency and robustness imposed by ECMWF's various global operational applications and has the potential to form the basis of ECMWF's future non-hydrostatic dynamical core. The governing equations of this non-hydrostatic model are the unapproximated Euler equations for the (optionally) deep or shallow atmosphere (i.e. further approximations may be made to the rotating spherical system).

Testing framework

The tests performed ranged from seasonal climate runs at T159 (~125 km) to medium-range forecasts at T3999 (~5 km) to assess the performance of the non-hydrostatic model in the hydrostatic regime, all the way to idealised ultra-high resolution simulations in the non-hydrostatic regime (*Wedi et al.*, 2009). Experiments with the T2047 horizontal resolution indicate that the differences between the hydrostatic and the non-hydrostatic simulations are still not significant at this resolution.

Even the finest horizontal resolution at which the IFS can be run to date (T3999) is still too coarse to fully resolve non-hydrostatic phenomena. Consequently a test bed has been developed that enables testing of the global non-hydrostatic dynamical core at non-hydrostatic scales at an affordable computational cost. Rather than create a two-dimensional vertical slice model of the three-dimensional global model or develop a limited area version of the IFS, a testing framework more suited for the global code was considered.

The testing framework is based on the idea of shrinking the radius of the planet such that, with an affordable number of grid-points covering the globe, the desired resolution resolving non-hydrostatic phenomena is achieved, but without incurring the prohibitive cost associated with such a fine resolution on

the full-sized planet (*Wedi & Smolarkiewicz*, 2009). The size of the computational domain is reduced without changing the depth or the vertical structure of the atmosphere. The underlying assumption is that the essential flow characteristics remain unchanged when the ratio of horizontal to vertical scales is reduced. Consequently, the planetary radius is suitably reduced to capture non-hydrostatic phenomena without incurring the computational cost of actual simulations of weather and climate at non-hydrostatic resolution.

It is desirable to directly compare, both quantitatively and qualitatively, non-hydrostatic simulations with analytic solutions and with large-eddy simulation (LES) benchmarks of limited-area models published in the literature. The following sections describe a selection of examples using small-planet simulations that illustrate the difference between hydrostatic and non-hydrostatic simulations while assessing the efficacy of the non-hydrostatic IFS model in more detail.

Orographically-forced gravity waves

An example that illustrates the difference between hydrostatic and non-hydrostatic models is the propagation of orographically-forced gravity waves in the presence of vertical wind shear. In this case consider the flow over a mountain with a height of 100 m in a vertically stratified atmosphere with constant Brunt-Väisälä frequency and with the wind linearly increasing from 10 ms^{-1} at the surface to 35 ms^{-1} at the tropopause and then constant aloft. The reference solution (Figure 1a) is provided by the state-of-the-art model EULAG (*Prusa et al.*, 2008). This shows trapped, horizontally-propagating gravity waves.

Figures 1b and 1c show the non-hydrostatic and the hydrostatic solutions from the IFS. While the hydrostatic model produces vertically-propagating mountain gravity waves, the non-hydrostatic version correctly generates the trapped, horizontally-propagating gravity waves. The image in Figure 2 shows an example of such wave motions – likely to be misrepresented in a hydrostatic model – off Amsterdam Island in the southern Indian Ocean. The ship-wave like banded cloud structures are stretching far leeward of the island. The corresponding observed vertical wind shear that is necessary to guide the gravity waves in the horizontal direction is shown in Figure 3, as analysed by ERA-Interim.

Other examples that test the veracity of the IFS model using the unapproximated Euler equations range from horizontally- and vertically-propagating spherical acoustic waves, through 'local-scale' orographically forced gravity waves in the presence of shear and critical levels, to 'global-scale' planetary Rossby waves in idealised global-scale simulations. The interested reader can find further information in *Wedi et al.* (2009) and references therein.

Explicit deep convection

The previous example has been run using only the dynamical core of the IFS model. In IFS the physical parametrizations ('physics') are computed separately from the dynamical core ('dynamics') of the model (apart from the change of air density due to moist quantities and their advection by the wind). Therefore, this section focuses on cloud simulations

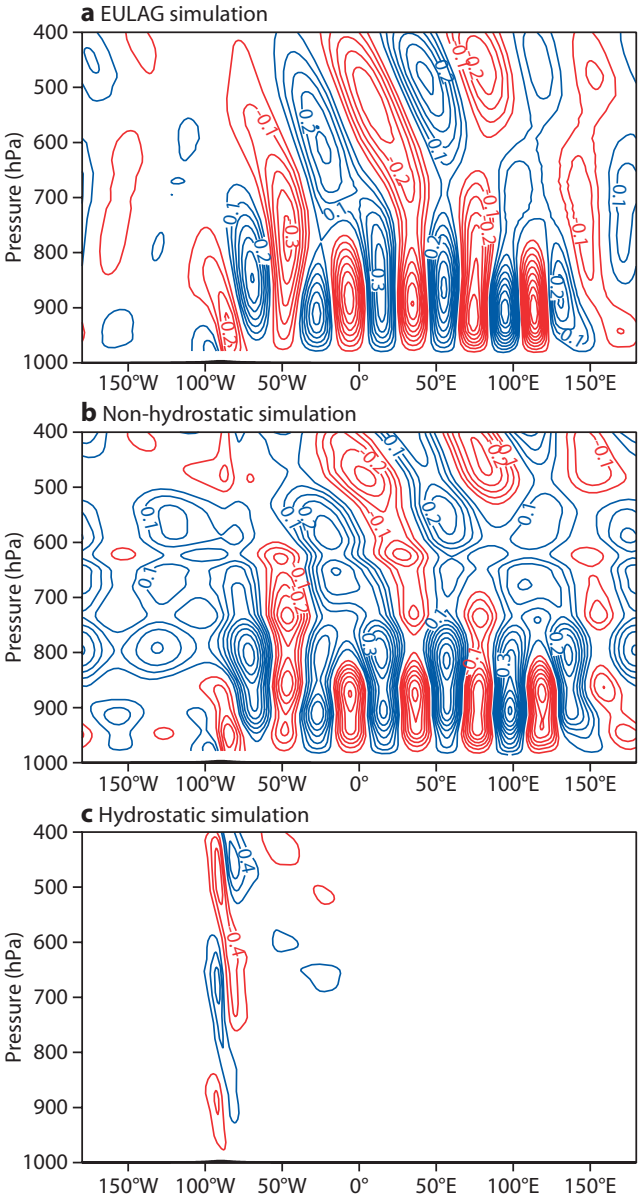

Figure 1 Vertical cross-section at the equator of vertical velocity comparing (a) the non-hydrostatic EULAG simulation with (b) non-hydrostatic and (c) hydrostatic IFS simulations for a linearly-sheared flow past a quasi-two-dimensional 'witch of Agnesi' obstacle at the equator on the reduced-size sphere. The atmosphere is vertically-stratified (Brunt-Väisälä frequency $N = 0.01\ s^{-1}$) and there is a zonal flow of 10 ms^{-1} impinging on the mountain near the surface, increasing linearly to 35 ms^{-1} at 10.5 km (or approximately 687 hPa) and constant above. Contour interval is 0.05 ms^{-1}; blue/red lines denote positive/negative contours.

on the reduce-size planet, with an emphasis on sensitivities regarding hydrostatic versus non-hydrostatic dynamics.

Theoretical considerations

The prognostic evolution of the vertical velocity in the non-hydrostatic system of equations (as opposed to the diagnostic determination of vertical velocity in the hydrostatic equations) is required to adequately describe the vertical accelerations in deep convective clouds and buoyancy-driven gravity waves triggered by convection. To resolve deep convective clouds

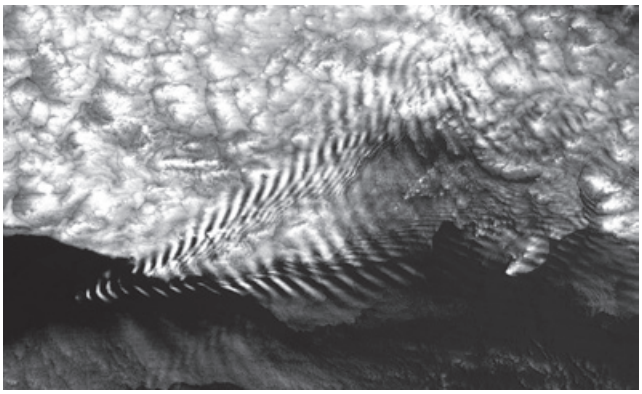

Figure 2 NASA satellite image (MODIS imager on board the Terra satellite) of a trapped lee wave forming off Amsterdam Island. Image taken on 19 December 2005.

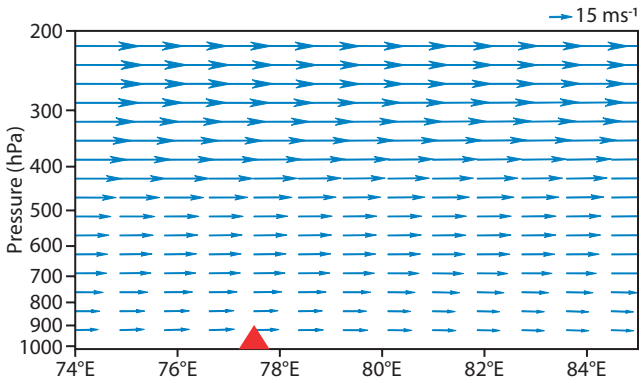

Figure 3 Vertical cross-section at 37.8°S of analysed ERA-Interim winds on 19 December 2005. The location of Amsterdam Island is indicated by the red marker.

(Cumulonimbus, Nimbostratus) a resolution at least of order 2 km is needed.

The development of a deep convective cloud is due to a positive feedback between the vertical motion, determined by the non-hydrostatic momentum equation, and the (microphysical) parametrization of condensation in the physics. With a grid interval of order 10 km and using a hydrostatic model such processes are entirely sub-grid scale and a deep convection parametrization is required instead.

It is worth noting that there is a common perception that a hydrostatic model cannot reproduce the high vertical velocities found in a deep convective cloud. To the contrary, the vertical velocity in convective updrafts, diagnosed from a hydrostatic model used with a grid interval of order 2 km, is usually stronger than the vertical velocity predicted by the non-hydrostatic model. The classical explanation is that the non-hydrostatic model accurately describes the transient stage during which the ascending air has to 'push' the air above and is slowed down in the process. In contrast, in a hydrostatic model the air is supposed to reach a hydrostatic equilibrium instantaneously thus neglecting the effect of deceleration. Based on these considerations, it should now be apparent that, despite some success of hydrostatic models in modelling motions at increasingly finer grid intervals, the hydrostatic equations are an approximation that is no longer justified for resolved atmospheric scales of order 10 km or less.

Simulation of explicit deep convection

One of the first tests used to validate a model for explicit deep convection is to simulate the ascent of warm and/or moist bubbles. The air in the grid boxes included in the bubble is positively buoyant compared to the air in the grid boxes outside the bubble. If the bubble reaches its level of neutral buoyancy before being saturated, the bubble decelerates and the ensuing oscillation around its level of neutral buoyancy excites gravity waves. But if the level of condensation is reached, the vertical motion of the bubble may continue up to the tropopause due to the warming associated with latent heat release of cloud formation.

With the small planet configuration, a T159 resolution on a planet with a radius of 64 km has a horizontal resolution of about 1.25 km. Dry and moist bubbles triggered by a low-level warming near the equator of the small planet in an initial no-wind environment are rising to their level of neutral buoyancy. When the condensation scheme of the current ECMWF physics is activated, the updraft reaches the tropopause and a large cloud develops (Figure 4). Even with these relatively simple microphysics of clouds and precipitation (no airborne rain or snow), the model reproduces the feedback between the vertical acceleration and the warming due to condensation, both in the hydrostatic and the non-hydrostatic simulation.

The cloud in the hydrostatic simulation appears after 25 min (Figure 4a). Yet after a further 10 min of cloud development, the hydrostatic model produces unrealistic vertical velocities of more than 60 ms^{-1} in the centre of the updraft. The cloud in the non-hydrostatic simulation appears later (after 35 minutes), and vertical velocities do not reach more than 30 ms^{-1} (Figure 4b). These results show that the hydrostatic model develops a faster, more intense cloud and also spreads the cloud more horizontally than in the non-hydrostatic simulation.

The cooling resulting from the evaporation of the precipitation underneath the cloud creates resolved downdrafts which spread out into density currents near the surface. In this low-wind environment, the density currents isolate the convective ascent from its low-level moist inflow and the main cloud starts to dissolve after about 15 minutes of development in both simulations. The density currents trigger new ascents on the sides and smaller clouds develop as the main cloud decays – see the bottom panels in Figure 4.

Other implications for the IFS model

When the IFS is used at resolutions permitting the mechanisms for explicit deep convection, this type of – albeit very idealised – simulations is useful to validate the numerical algorithms (e.g. semi-Lagrangian advection, semi-implicit time stepping or the impact of the spectral transforms), investigate the coupling between the physics and the dynamics, and evaluate the effect of additional prognostic quantities such as rain or snow.

As water vapour is the 'main fuel' of deep convection, the local conservation of hydrometeors is very important for a correct simulation of explicit deep convection. However, as the IFS semi-Lagrangian advection scheme is neither conservative nor strictly preserves monotonicity, especially near

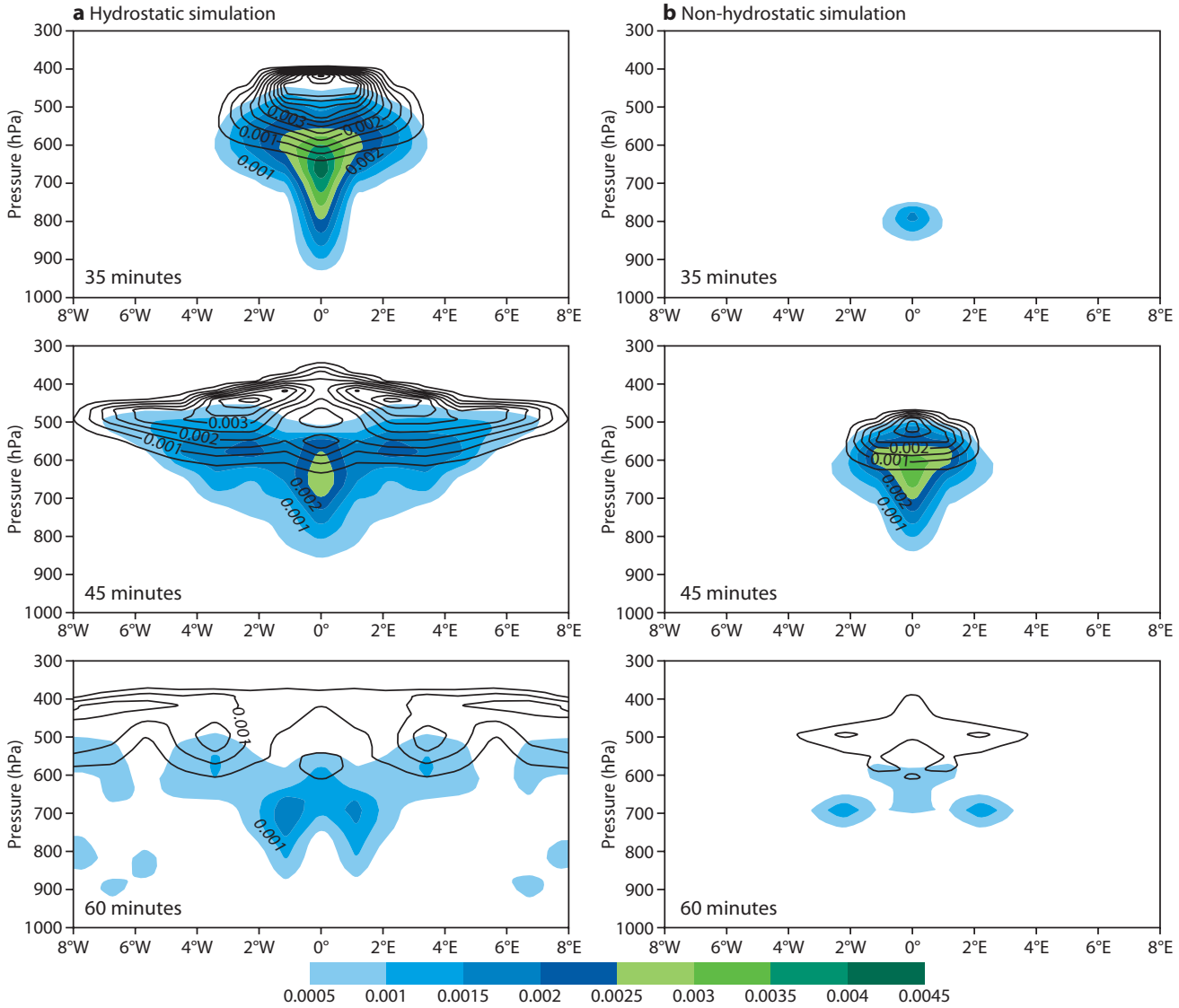

Figure 4 Vertical cross-sections along the equator showing the evolution of the cloud liquid water content (shading, kg/kg) and the cloud ice water content (black contours, kg/kg) in (a) hydrostatic and (b) non-hydrostatic simulation after 35, 45 and 60 minutes.

regions of sharp gradients like the tropopause or near the surface, spurious sources of water or potentially warm or cold air may appear and dramatically change the buoyancy of the bubbles. Therefore, modifications to the semi-Lagrangian advection are investigated to remedy this shortcoming.

The recent advances in the development of prognostic microphysics (available in the IFS from cycle 36r4) will allow more sophisticated test cases of idealised squall lines and tropical cyclones in the future. These simulations will be run on the small planet and complemented with selected simulations at ultra-high resolution (in the non-hydrostatic regime) to study also the interaction of deep convective updrafts with tropical waves and their mesoscale convective organisation.

Ultra-high resolution global weather forecasts

The limits of the existing software and hardware capabilities have been explored by conducting the first T3999 global 24-hour forecasts with the IFS in its operational configuration. Figure 5 shows a comparison of the cloud cover distribution over the Scandinavian Peninsula for the non-hydrostatic (Figure 5a) and the hydrostatic (Figure 5b) T3999 simulations. Differences are starting to appear, in particular leeward of mountains due to the aforementioned influence of orographically-forced gravity waves, although the overall patterns are still very similar with a substantial accumulation of clouds in the blocked flow region upwind of the Scandinavian Peninsula ('Staubewölkung'). At this resolution (5 km grid interval) each prognostic variable has approximately 21 million points per vertical level. It takes approximately 50 minutes using 128 nodes (i.e. half of one of the IBM clusters installed at ECMWF) to produce a 24-hour forecast. The results are very reasonable with substantially more topographic detail compared to the current operational T1279 (~16 km) resolution.

While challenging ECMWF's infrastructure in many ways (e.g. post-processing, archiving and plotting – many thanks to Manuel Fuentes, Sylvie Lamy-Thépaut and Fernando Ii), most importantly this feasibility study emphasises the importance of efficient spectral transforms (see Box A for more details) and the associated efficacy of the non-hydrostatic

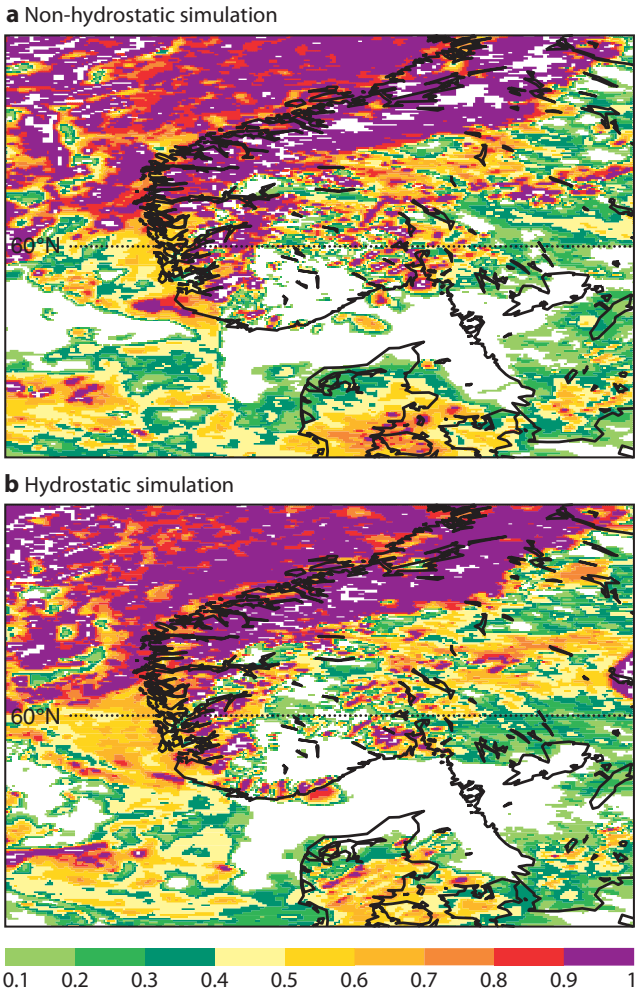

Figure 5 Comparison of the cloud cover for (a) non-hydrostatic and (b) hydrostatic IFS forecasts for 17 March 1998 at T3999 (~5 km) resolution, with a north-westerly flow impinging on the Scandinavian Peninsula. The differences in the cloud cover between the two simulations may be attributed to the different representation of the flow over the mountainous regions in the presence of wind shear.

code framework. The latter arises because of the likely need to change from the hydrostatic to the non-hydrostatic IFS at 5 km resolution. Doubling the resolution from approximately 10 to 5 km comes therefore with a substantial change in the way each part of the model contributes to the cost of a single time-step and with an increase of the total cost. The current version of the non-hydrostatic IFS model takes approximately three times longer at T3999 resolution (2.5 hours for a 24-hour forecast) due to the increased number of spectral transforms required for a numerically stable model integration.

Future developments

Current research at ECMWF focuses on:

- Exploring recent developments of 'Fast Legendre Transforms' aimed at reducing the number of calculations required in the spectral transforms.
- Reducing the number of transforms required by exploring *a priori* filtering of acoustic waves (i.e. sound-proofing of the governing equations).

Also further developments are planned with a focus on the dynamics-physics coupling and the accuracy of the semi-Lagrangian advection scheme to prepare for the transition from parametrized to cloud-resolving simulations.

A workshop held at ECMWF (8–10 November 2010) brought together leading experts in the field of non-hydrostatic modelling to discuss recent developments in this area and to provide further recommendations on how to prepare the IFS for global atmospheric modelling at future high to ultra-high resolutions.

Finally, given the increased sensitivity to topographic detail at the targeted resolutions where non-hydrostatic effects matter, a separate project is under way with a view to replacing the topographic maps underlying ECMWF's current operational weather forecasts with the latest available satellite-derived products.

The spectral transform method

A

The spectral transform method has been successfully applied at ECMWF for approximately thirty years. It involves discrete spherical harmonics transformations between physical (grid point) space, where the semi-Lagrangian advection and the physical parametrizations are computed, and spectral (spherical harmonics) space, where the Helmholtz equation – arising from the semi-implicit scheme – can be solved easily and horizontal gradients are computed accurately. A spherical harmonics transformation is a Fourier transformation in longitude and a Legendre transformation in latitude.

The Fourier transform is computed numerically very efficiently by using the Fast Fourier Transform (FFT). However, due to the relative cost increase of the Legendre transforms compared to the grid point computations, very high-resolution spectral models may become prohibitively expensive. For the hydrostatic model at a horizontal resolution of T2047 (10 km) the computational cost of the spectral transforms in terms of total floating point operations per time-step is about 50% of the total. Yet, due to the very high level of optimisation achieved for the spectral computations, the transforms only contribute less than 20% to the elapsed time at T2047 resolution.

FURTHER READING

Bénard, P., J. Vivoda, J. Mašek, P. Smolíková, K. Yessad, C. Smith, R. Brožková & J-F. Geleyn, 2010: Dynamical kernel of the ALADIN-NH spectral limited-area model: Revised formulation and sensitivity experiments. *Q. J. R. Meteorol. Soc.*, **136**, 155–169.

Prusa, J.M., P.K. Smolarkiewicz & A.A. Wyszogrodzki, 2008: EULAG, a computational model for multiscale flows. *Comput. Fluids*, **37**, 1193–1207.

Wedi, N.P. & P.K. Smolarkiewicz, 2009: A framework for testing global nonhydrostatic models. *Q. J. R. Meteorol. Soc.*, **135**, 469–484.

Wedi, N.P., K. Yessad & A. Untch, 2009: The nonhydrostatic global IFS/ARPEGE: model formulation and testing. *Tech. Report No. 594*, ECMWF, Reading, UK.

Prediction of extratropical cyclones by the TIGGE ensemble prediction systems

LIZZIE S. R. FROUDE
Environmental Systems Science Centre,
University of Reading, UK

EXTRATROPICAL CYCLONES are fundamental to the everyday weather in the mid-latitudes, but they can also be extremely hazardous. The accurate prediction of these weather systems is therefore of key importance. A cyclone tracking technique has been developed for analysing the prediction of extratropical cyclones by numerical weather prediction. This technique has been used to compare the prediction of extratropical cyclones by nine different Ensemble Prediction Systems (EPSs). These will be identified by just the name of the production centre (see Box A). These EPS data are freely available to researchers via the THORPEX Interactive Grand Global Ensemble (TIGGE) archives (see *Bougeault et al.*, 2010).

Results show large differences in cyclone predictive skill between the different EPSs. Key findings include:

- ECMWF has the highest level of skill in predicting cyclone position, intensity and propagation speed.
- The Japan Meteorological Agency (JMA), the National Centers for Environmental Prediction (NCEP), the Met Office (UKMO), and the Canadian Meteorological Centre (CMC) have the next highest level of skill.
- NCEP, the Centro de Previsão de Tempo e Estudos Climáticos (CPTEC), and the Australian Bureau of Meteorology (BoM) significantly underpredict cyclone intensity. They also have faster intensity error growth in the earlier part of the forecast and are very underdispersive in cyclone intensity.
- Cyclone propagation speed is underpredicted (i.e. the forecast cyclones propagate slower than the analysed cyclones) by the perturbed members and control forecasts of all nine EPSs.
- For all nine EPSs, the ensemble mean provides very little advantage over the control forecast for cyclone position, but for cyclone intensity the ensemble mean does provide a significant improvement.
- ECMWF and JMA have an excellent spread-skill relationship for cyclone position in the northern hemisphere and ECMWF also does in the southern hemisphere. The other EPSs are underdispersive.
- All the EPSs are much more underdispersive for cyclone intensity. ECMWF and CMC have the smallest difference between ensemble spread and ensemble mean error.

This article briefly describes the methodology used to analyse the TIGGE data and discusses some of the results. For further details the reader is referred to *Froude* (2010a,b).

The nine centres whose EPSs have been used in this study **A**

- Bureau of Meteorology (BoM)
- Canadian Meteorological Centre (CMC)
- Centro de Previsão de Tempo e Estudos Climáticos (CPTEC)
- China Meteorological Administration (CMA)
- European Centre for Medium-Range Weather Forecasts (ECMWF)
- Japan Meteorological Agency (JMA)
- Korea Meteorological Administration (KMA)
- National Centers for Environmental Prediction (NCEP)
- UK Met Office (UKMO)

Note that Météo-France is excluded from the analysis because its forecasts are only integrated out to three days, which is not long enough to include the full life cycle of a large number of cyclones.

TIGGE data and storm tracking methodology

Medium-range ensemble forecasts are now routinely produced at numerous operational weather centres around the world. The EPSs of these centres differ in many ways, using different models, resolutions, perturbation methodologies and so on. It is important to assess and compare the performance of the different EPSs to determine the impact the different configurations have on forecast performance and to determine how the EPSs could be improved.

TIGGE is a major component of the World Weather Research Programme. One of its main objectives is to enhance collaboration on the development of ensemble prediction between operational centres and universities by increasing the availability of EPS data for research. Since 1 February 2008 ten operational weather forecasting centres have been delivering near-real-time ensemble forecast data to three TIGGE data archives located at ECMWF, the National Center for Atmospheric Research (NCAR) and the China Meteorological Administration (CMA). For further details of TIGGE see *Bougeault et al.* (2010).

The prediction of extratropical cyclones by nine of the EPSs contained in the TIGGE archives has been assessed. Table 1 lists these EPSs and summarises their main characteristics.

Extratropical cyclones are identified and tracked using 850 hPa relative vorticity field separately in the northern (20°–90°N) and southern (20°–90°S) hemispheres for all perturbed members and control forecasts. This identification and tracking is also performed with the ECMWF analysis. Cyclones predicted by the different EPSs are compared with those in the ECMWF analysis, and forecast verification diagnostics are generated for

Centre	Horizontal resolution	Number of levels	Number of members	Initial perturbations	Perturbation of model physics	Forecast length (days)	Forecast base times (UTC)	Data assimilation
BoM (Australia)	TL119 (1.5°)	19	32	SVs (NH, SH)	No	10	00, 12	GenSI
CMA (China)	T213 (0.5625°)	31	14	BVs (Globe)	No	10	00, 12	GSI
CMC (Canada)	TL149 (1.2°)	28	20	EnKF (Globe)	Yes	16	00, 12	4D-Var
ECMWF (Europe)	TL399 (0.45°) TL255 (0.7°)	62	50	SV (Globe)	Yes	0–10 10–15	00, 12	4D-Var
JMA (Japan)	TL319 (0.5625°)	60	50	SVs (NH, TR)	No	9	12	4D-Var
KMA (Korea)	T213 (0.5625°)	40	16	BVs (NH)	No	10	00, 12	3D-Var
NCEP (USA)	T126 (0.9474°)	28	20	ET (Globe)	No	16	00, 06, 12, 18	GSI
UKMO (UK)	1.25°×0.83°	38	23	ETKF (Globe)	Yes	15	00, 12	4D-Var
CPTEC (Brazil)	T126 (0.9474°)	28	14	EOF (45°S–30°N)	No	15	00, 12	NCEP Anal

Table 1 Characteristics of the nine EPS used in this study. The abbreviations used in the table are as follows; SV (Singular Vector), BV (Bred Vector), ET (Ensemble Transform), EnKF (Ensemble Kalman Filter), ETKF (Ensemble Transform Kalman Filter), EOF (Empirical Orthogonal Functions), NH (Northern Hemisphere), SH (Southern Hemisphere), TR (Tropics), GenSI (Generalised Multivariate Statistical Interpolation), 3/4D-Var (3/4 Dimensional Variational Analysis), GSI (Gridded Statistical Interpolation), Tx (spectral triangular truncation at total wave number x) and TLx (spectral triangular truncation at total wave number x with linear grid). (From *Froude*, 2010a).

cyclone position, intensity and propagation speed. Since the cyclones are verified against the ECMWF analysis, there may be some positive bias towards ECMWF in the results. However, previous work suggests this will only be significant in the earlier part of the forecast. Further details of the cyclone identification and tracking methodology are provided in Box B.

An Atlantic cyclone

Figure 1a shows an example of the tracks and intensities of an Atlantic cyclone predicted by ECMWF. The analyzed Atlantic cyclone (shown in black) formed over North America at 00 UTC on 22 February 2008. It then travelled across the Atlantic, intensifying rapidly over the next three days before reaching its maximum relative vorticity amplitude of $11.9\times10^{-5}\ s^{-1}$ at 06 UTC on 25 February. The cyclone then moved north of the British Isles, over Scandinavia, and just into Russia while decaying over the next 3.5 days.

The ensemble member tracks are tightly spaced around the analysis track indicating that this particular cyclone is highly predictable. The mean track (calculated by averaging all the ensemble member tracks) and the control track lie virtually on top of each other until day 4 of the forecast. From this point the control track is slightly too far to the south and the mean is closer to the analysis. The spread in the intensity for this cyclone is also small, particularly during the initial growth phase in the first day of the forecast. From this point the ensemble members are more dispersed. Both the ECMWF control and ensemble mean exhibit high levels of predictive skill for this cyclone.

Figures 1b and 1c show the control tracks/intensities and mean tracks/intensities respectively for each of the nine EPSs. The track of the cyclone is predicted very well by all the centres until about day 4, when (as with ECMWF) the forecast tracks begin to diverge from the analyzed track. Some of the forecast cyclones travel considerably farther into Russia than the analyzed cyclone. There is a larger difference in performance between the centres for the cyclone's intensity than track. Overall ECMWF and Korea Meteorological Administration (KMA) have the highest level of performance. The CMA mean and control overpredict the maximum intensity of the cyclone and the other centres have an underprediction.

For this particular cyclone there is only a small difference in skill between the control and ensemble mean. However, for other cyclones, there can be a larger difference. The

Cyclone tracking methodology B

The cyclones are identified and tracked along the 6-hourly forecast trajectories of each of the perturbed ensemble members, the control forecasts and analysis data using the method of *Hodges* (1995, 1999). The cyclones are identified in the 850-hPa relative vorticity field. In order that only synoptic-scale extratropical cyclones are identified, the data is first reduced to a resolution of T42. The planetary scales with total wave numbers less than or equal to 5 are also removed as in *Hoskins & Hodges* (2002). Once the cyclones are identified the tracking is performed by the minimisation of a cost function. Only those cyclone tracks that last at least 2 days and travel further than 1000 km are retained for the statistical analysis.

A matching methodology is used to objectively determine which forecast tracks correspond to which analysis tracks. A forecast cyclone track was considered to be the same system as an analysis cyclone track (i.e. matched) if the two tracks met certain predefined spatial and temporal criteria (see *Froude*, 2010a for details). The forecast tracks that matched with analysis tracks are then used to compute diagnostics for cyclone position, intensity and propagation speed.

As with any analysis methodology there may be biases and shortcomings that have some impact on the results. For further details and discussion of this please see *Froude et al.* (2007).

relative performance of the different EPSs can also vary considerably for different cyclones (see *Froude*, 2010a). This highlights the importance of performing a statistical analysis of a large number of cyclones to assess the skill and determine the strengths and weaknesses of the different EPSs.

Comparison of ensemble mean skill

Figure 2 shows the ensemble mean error in cyclone position, intensity and propagation speed for each EPS in the northern and southern hemispheres for the 6-month period from 1 February to 31 July 2008. For details of how the ensemble mean error is calculated see Box C. There is a large difference in forecast skill between the different EPSs. ECMWF has the highest level of skill for all cyclone properties, with NCEP, JMA, UKMO and CMC having the next highest level of performance.

NCEP, CPTEC and BoM have faster initial error growth in cyclone intensity than the other EPSs (Figure 2b). This is perhaps because these EPSs have comparatively low resolutions and are not able to accurately capture the cyclones' growth and decay. CMC is also integrated at a comparatively low resolution and does not exhibit this rapid intensity error growth. However, unlike NCEP, CPTEC and BoM, CMC has a 4D-Var data assimilation system. Perhaps this is compensating for the low resolution by providing a better initial state.

The errors in the southern hemisphere are larger than in the northern hemisphere for all the EPSs, but CMA and KMA have significantly larger errors in the southern hemisphere compared to the northern hemisphere. This is perhaps to be expected for KMA since it does not apply perturbations in the southern hemisphere. For CMA (which does apply pertur-

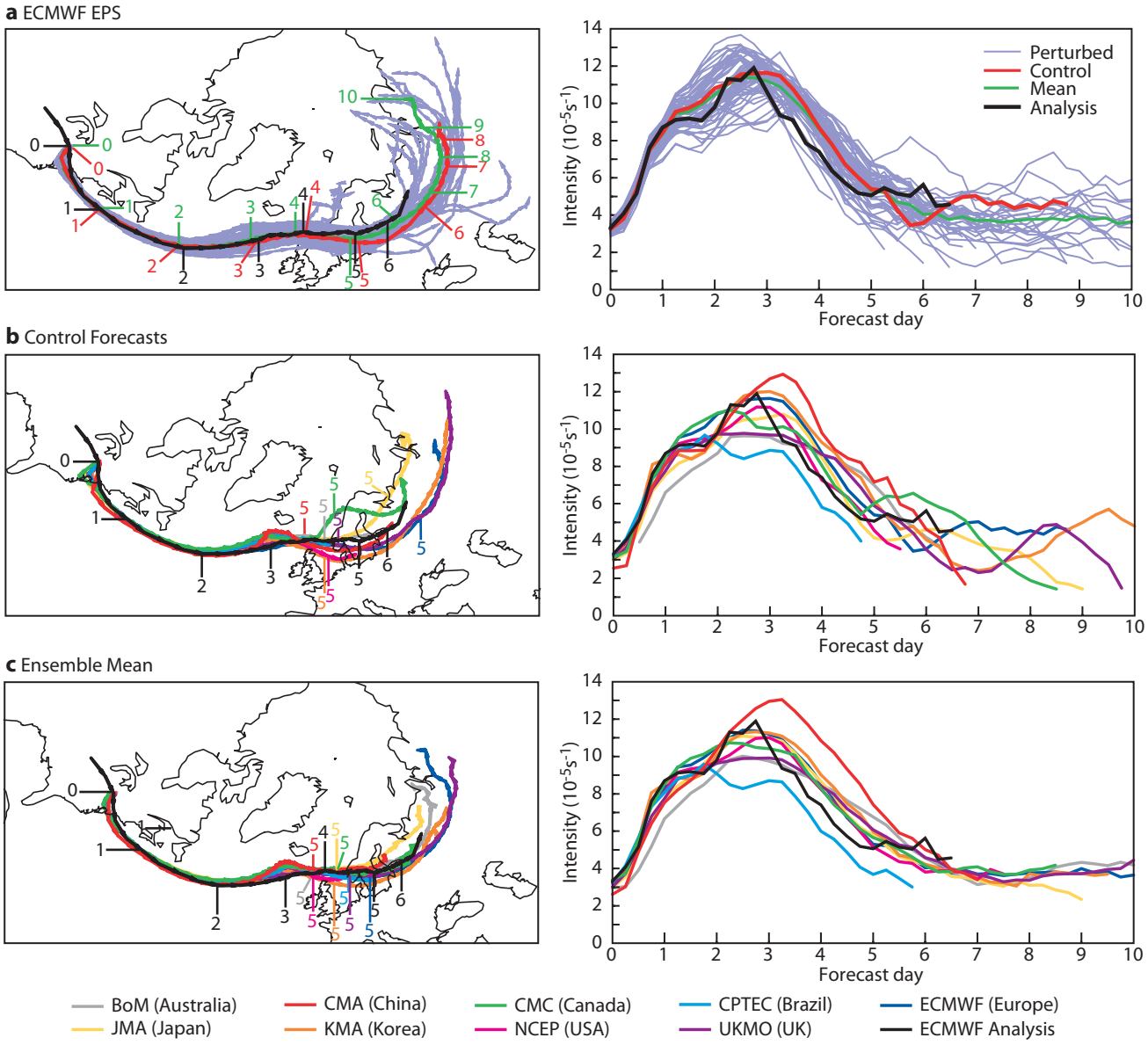

Figure 1 Tracks and intensities of an Atlantic cyclone predicted by the (a) ECMWF EPS, (b) control forecasts of each EPS and (c) ensemble mean (calculated by averaging all the ensemble member tracks/intensities) of each EPS. The ECMWF analysis is also shown in all the plots. Units of intensity are 10^{-5} s^{-1} (relative to background field removal) and the numbers along the tracks correspond to the forecast lead-time in days. The forecast start time (day 0) is 12 UTC on 22 February 2008. (Figure partly from *Froude*, 2010a).

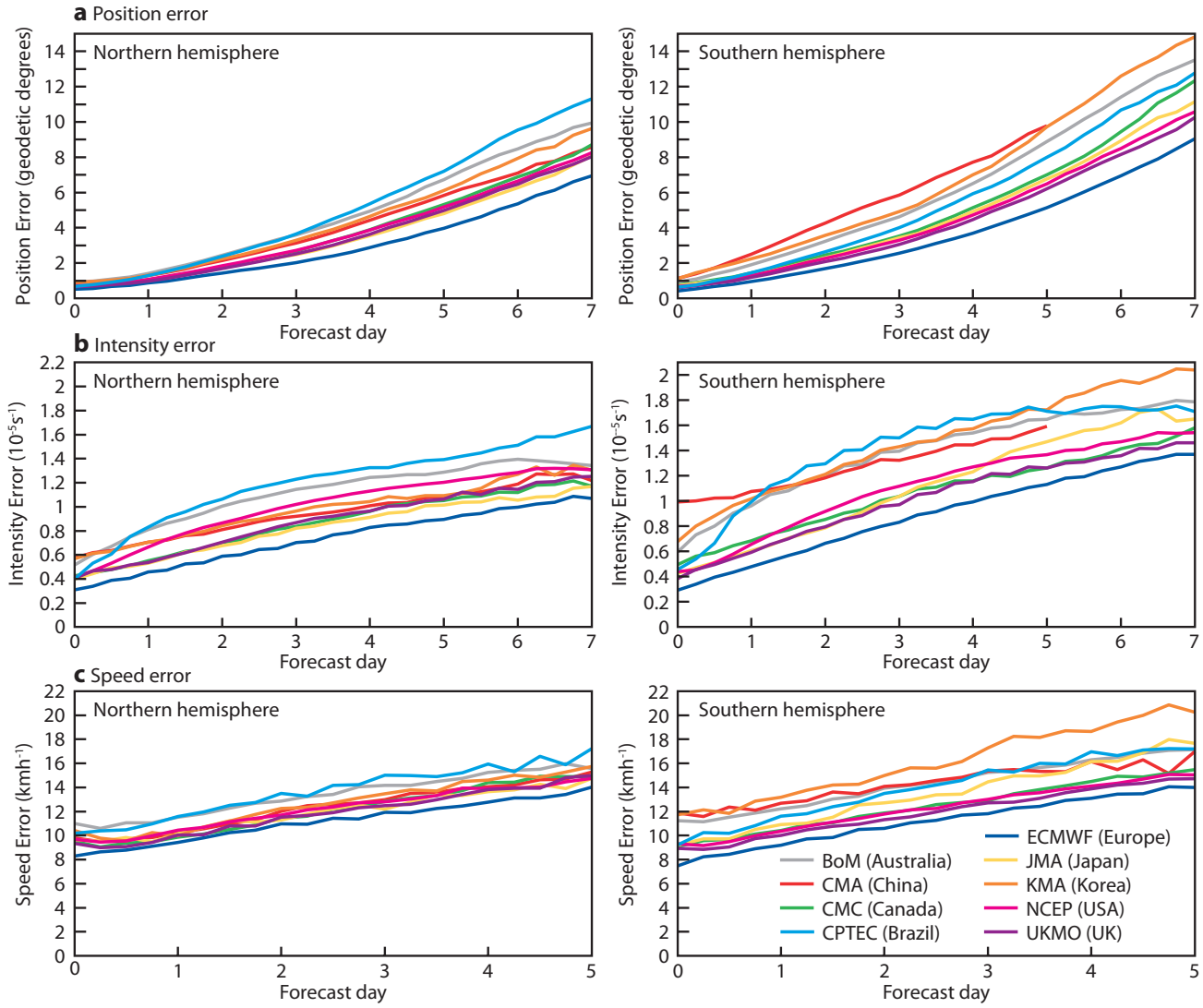

Figure 2 EPS mean error in (a) position, (b) intensity and (c) propagation speed in the northern (left) and southern (right) hemispheres for 1 February to 31 July 2008. The curves are only plotted to day 5 for the CMA EPS in the southern hemisphere due to insufficient matches between forecast and analysis tracks (see *Froude*, 2010b). The intensity is assessed relative to background field removal. (Figure from *Froude*, 2010b).

bations in both hemispheres) the difference in the error between hemispheres is particularly noticeable. The reason for this difference for CMA is less clear, but it is suspected that it is caused by large errors in the initial state, which are related to the observations used in this hemisphere and how they are assimilated (see *Froude*, 2010b for details).

The mean error in cyclone propagation speed is large throughout the forecast range for all EPSs (Figure 2c). It should be noted that the speed error is different in nature to the position or intensity error in that it would not necessarily be expected to grow with lead time (see Box C). However, there will be a cumulative effect of a consistent error in speed on the position of the cyclone with increasing lead-time.

Bias

Figure 3a shows the bias in the intensity error given in Figure 2b. CMC, ECMWF and JMA all have small biases, with ECMWF being the only one to consistently overpredict cyclone intensity. The magnitude of the ECMWF bias is slightly smaller in the southern hemisphere compared to the northern hemisphere. This is perhaps to be expected given the simpler more symmetric structure of this hemisphere in terms of land and sea, making cyclone development easier to model. It is apparent that CMA has a significantly larger positive bias at day 0 in the southern hemisphere compared to the northern hemisphere, but this bias becomes negative from day 2.5. As discussed above, this suggests a problem in the initial state of the CMA system.

BoM, NCEP, CPTEC and UKMO all significantly underpredict cyclone intensity. BoM, NCEP, and CPTEC in particular show a dramatic increase in negative bias in the earlier part of the forecast. This corresponds to the rapid error growth exhibited by these systems in the initial period (Figure 2b).

CPTEC has a significantly larger intensity bias in the southern hemisphere compared to the northern hemisphere. In particular there is a dramatic increase in negative bias in the first day of the forecast. This is most probably due to inconsistency between the initial state and forecast model since CPTEC

use NCEP's analysis as their initial state and run their own forecast model (see *Froude*, 2010b for further discussion).

Figure 3b shows the bias in the propagation speed error given in Figure 2c. Interestingly all the EPSs underpredict propagation speed (i.e. the predicted cyclone arrives too late). The magnitude of this bias is small, but the cumulative effect will result in the 5-day forecast being approximately 200–400 km behind the analysed cyclone, which would be of importance to many forecast users. CPTEC has a large jump in speed bias at the beginning of the forecast, which is again probably related to some type of adjustment of the model from the initial state.

Since all the EPSs have a negative bias in propagation speed and this bias was also found for the control forecasts (not shown) it must be related to the forecast models rather than the ensemble setup. To investigate this further, the propagation speed bias was also computed for ECMWF's deterministic (high resolution) forecast during the same period and is also shown in Figure 3b. During this time period the ECMWF deterministic forecast was run at a spectral resolution of T799 as opposed to T399 for the ECMWF EPS (see Table 1). The deterministic forecast has a smaller bias than the EPS. It appears that increasing the resolution of the forecast model decreases the bias. This is perhaps related to the temporal resolution of the ECMWF model, which is lower for the EPS (30 minutes) than the deterministic forecast (12 minutes).

Calculating the ensemble mean error C

The ensemble mean error is calculated by computing the mean track, mean intensity, and mean propagation speed of the matching ensemble member tracks (including the control) for each cyclone in each ensemble forecast at each forecast lead time.

The mean error in position is calculated as the mean geodetic separation distance between the mean tracks and the corresponding ECMWF analysis tracks. Also the mean intensity error was calculated similarly, from the filtered vorticity value (see Box A) at the cyclone centres, using the absolute intensity difference as the measure of error.

The propagation speeds of the analysis and ensemble member cyclones were calculated at each point on their tracks by comparing the position of consecutive points on the tracks. Since the points on the tracks are 6 hours apart, the speed calculated at each point corresponds to the average propagation speed of the cyclone in the next 6 hours.

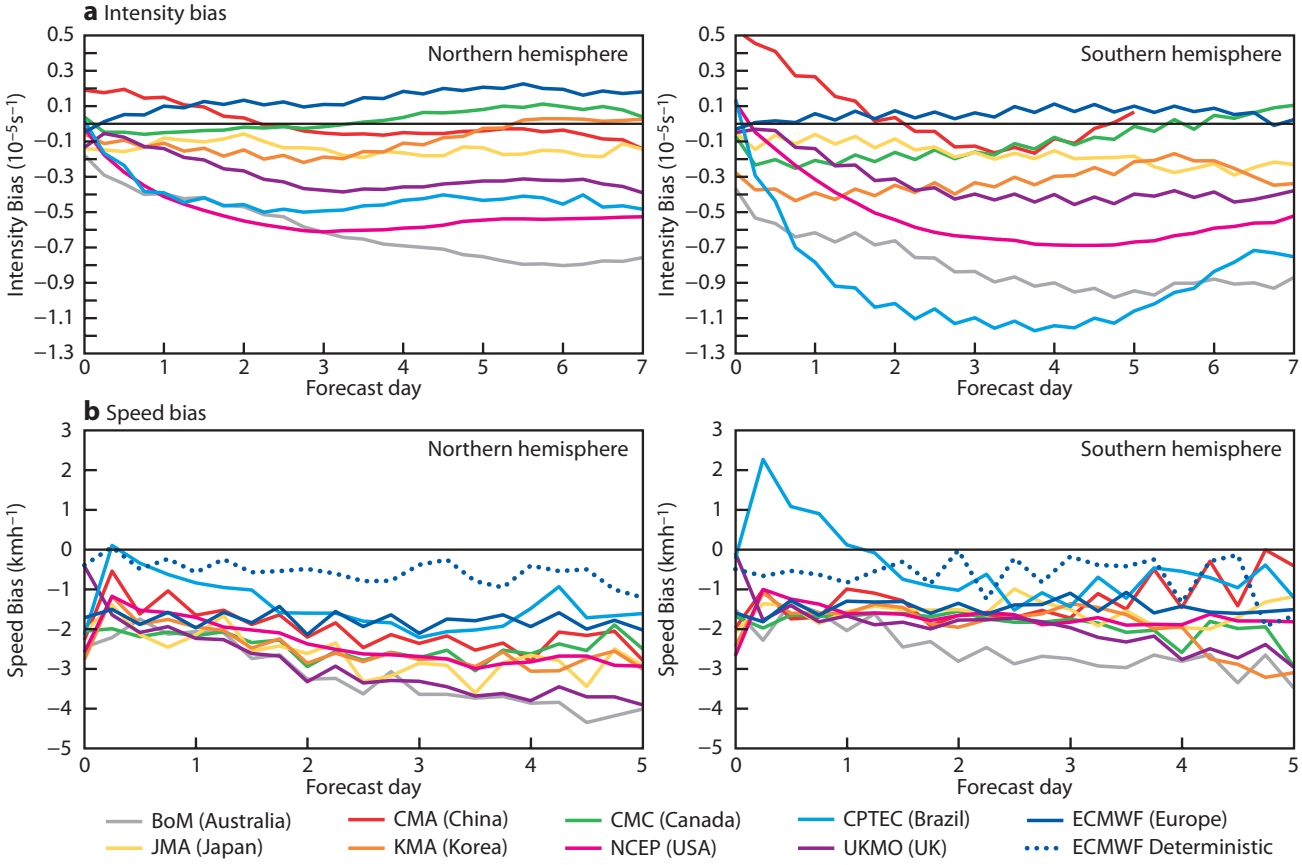

Figure 3 EPS mean bias in (a) intensity and (b) propagation speed in the northern (left) and southern (right) hemispheres for 1 February to 31 July 2008. The propagation speed bias is also shown for the ECMWF high-resolution deterministic forecast in (b). The intensity is assessed relative to background field removal. (Figure from *Froude*, 2010b).

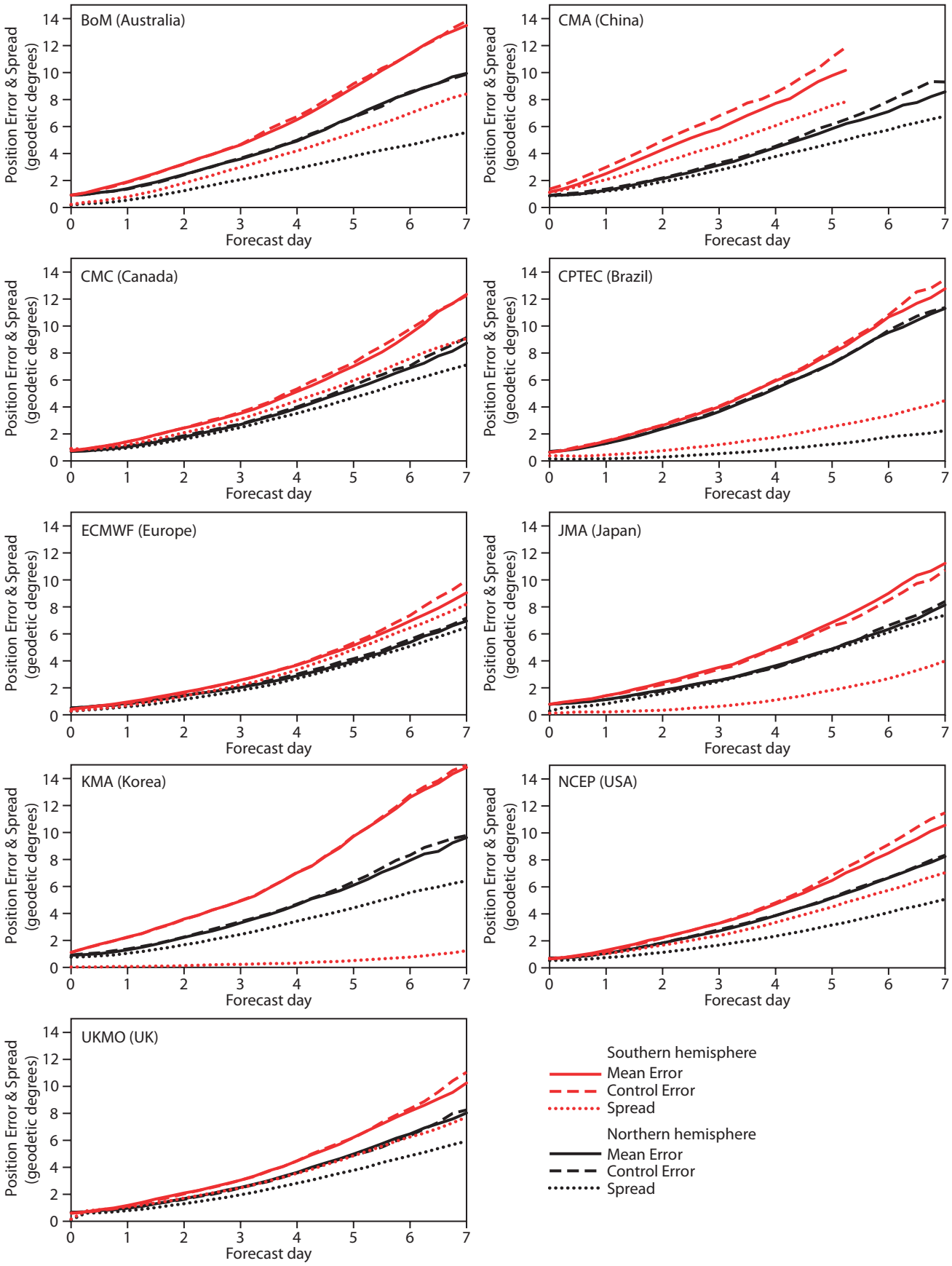

Figure 4 EPS mean error, control forecast error and spread in cyclone position for each EPS. The curves are only plotted to day 5 for the CMA EPS in the southern hemisphere due to insufficient matches between forecast and analysis tracks (see *Froude*, 2010b). (Figure from *Froude*, 2010b).

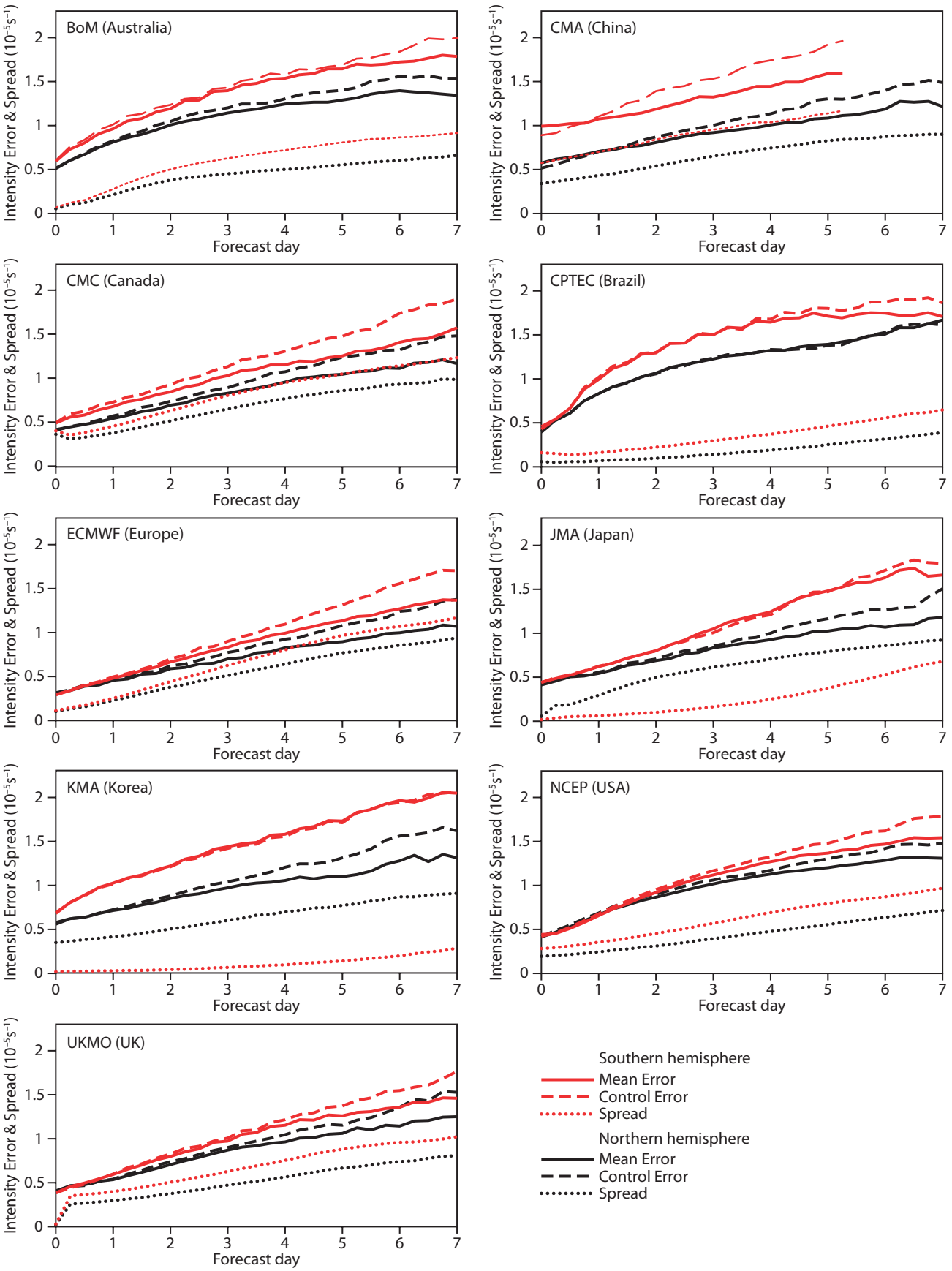

Figure 5 EPS mean error, control forecast error and spread in cyclone intensity for each EPS. The curves are only plotted to day 5 for the CMA EPS in the southern hemisphere due to insufficient matches between forecast and analysis tracks (see *Froude*, 2010b). The intensity is assessed relative to background field removal. (Figure from *Froude*, 2010b).

Mean error, control error and spread

Figures 4 and 5 show the ensemble mean error, control forecast error and ensemble spread, for cyclone position and intensity respectively, for each EPS and each hemisphere. Spread is calculated as the average distance of the ensemble member position/intensity from the analysis position/intensity. One of the aims of an EPS is for the ensemble mean to provide a forecast of higher skill than the control forecast.

It is clear that the ensemble mean provides very little advantage over the control forecast in predicting the position of cyclones for all EPSs (Figure 4). It is noted that a small difference can be seen for CMA in the southern hemisphere, but this is likely to be caused by insufficient data (see *Froude,* 2010b).

For the intensity of the cyclones, much more of a difference can be seen between the control and the ensemble mean (Figure 5). In the northern hemisphere the ensemble mean begins to provide an advantage over the control forecast for all the EPSs except CPTEC from around day 2. The results are similar in the southern hemisphere, except for JMA and KMA which do not apply perturbations in the southern hemisphere (see Table 1). The ensemble mean of these EPSs therefore provides no advantage over the control forecast.

For an EPS to be statistically reliable the spread should be equal to the ensemble mean error on average so that the spread can be used as a measure of the current predictability of the atmosphere, providing an estimate of the error in the ensemble mean forecast. In the northern hemisphere, ECMWF and JMA both have an excellent spread-skill relationship for cyclone position (Figure 4). This is interesting since the two systems have very similar characteristics in the northern hemisphere (see Table 1): both EPSs use 50 members, singular vector perturbations and 4D-Var, and have similar horizontal and vertical resolutions. There is however one major difference between the two systems in this hemisphere. ECMWF does include model perturbations whereas JMA does not, but this appears to have no impact on the spread-skill relationship for cyclone position. The other EPSs are all underdispersive to varying degrees. In the southern hemisphere, ECMWF also has an excellent spread-skill relationship for cyclone position. However, JMA and KMA are very underdispersive in the southern hemisphere, since they do not apply perturbations in this hemisphere.

For cyclone intensity (Figure 5) there are much larger differences between the spread and ensemble mean error for all EPSs. In the northern hemisphere the ECMWF and CMC have the highest performance, with JMA not performing quite as well. This is very interesting since ECMWF and CMC both perturb their forecast model physics. It seems that forecast model physics perturbations have more impact on increasing the spread in cyclone intensity than position. This is probably to be expected since cyclone position will be more dependent on the large-scale steering-level flow than on the smaller-scale parametrized processes that are perturbed. Cyclone intensity, on the other hand, will be much more influenced by these smaller-scale processes.

Future work

The cyclone tracking methodology provides useful information about the prediction of extratropical cyclones by EPSs and has revealed large differences in performance between the various systems. The relative performance of the EPSs varies for different measures of ensemble performance (i.e. forecast skill of the ensemble mean or the spread–skill relationship) and for the cyclone property (i.e. position or intensity). This highlights the importance of using a variety of verification measures when assessing the skill of a forecasting system.

Future work in the area of extratropical cyclone predictability will focus on the following key areas.

- ***Regional analysis***: The differences in predictive skill of cyclones in different regions by the EPSs will be assessed.
- ***Vertical structure***: The vertical structure and tilt of cyclones will be explored to gain a more in-depth understanding of the impacts that different factors, such as resolution, have on the prediction of cyclone growth and evolution.
- ***Forecast users***: The results and cyclone-tracking methodology of this article are potentially very useful to a wide range of forecast users. However, further work is required to determine how the results should be interpreted and utilized by each particular user. Forecast tools will be developed to present storm prediction information to users in the marine and insurance sectors.
- ***Other types of weather system***: The cyclone identification and tracking methodology is flexible and can be applied to other types of weather systems such as polar lows and tropical cyclones. The predictability of these other types of weather system will be explored.

The author would like to thank Kevin Hodges, Robert Gurney and Lennart Bengtsson for their help and advice on this work and the TIGGE contribution centres and data centres are acknowledged for providing the EPS data.

FURTHER READING

Bougeault, P. & Co-authors, 2010: The THORPEX Interactive Grand Global Ensemble (TIGGE). *Bull. Am. Meteorol. Soc.*, **91**, 1059–1072.

Froude, L.S.R., 2010a: TIGGE: Comparison of the prediction of northern hemisphere extratropical cyclones by different Ensemble Prediction Systems. *Weather and Forecasting*, **25**, 819–836.

Froude, L.S.R., 2010b: TIGGE: Comparison of the prediction of southern hemisphere extratropical cyclones by different Ensemble Prediction Systems. *Weather and Forecasting*, submitted.

Froude, L.S.R., L. Bengtsson & K.I. Hodges, 2007: The Predictability of extratropical storm tracks and the sensitivity of their prediction to the Observing System. *Mon. Wea. Rev.*, **135**, 315–333.

Hodges, K.I., 1995: Feature tracking on the unit sphere. *Mon. Wea. Rev.*, **123**, 3458–3465.

Hodges, K.I., 1999: Adaptive constraints for feature tracking. *Mon. Wea. Rev.*, **127**, 1362–1373.

Hoskins, B.J. & K.I. Hodges, 2002: New perspectives on the northern hemisphere winter storm tracks. *J. Atmos. Sci.*, **59**, 1041–1061.

Metview Macro – A powerful meteorological batch language

STEPHAN SIEMEN, FERNANDO II, IAIN RUSSELL

PARALLEL TO its graphical user interface (GUI), Metview offers a high-level meteorological scripting language to describe the retrieval, processing and visualisation of meteorological data. A scripting language was part of the first design specification of Metview and has always been an integral part. A language is the best 'user interface' to describe complex sequences of actions, particularly if the flow of action is conditional; this includes the expression of mathematical formulae and other forms of data manipulation.

The philosophy behind Metview Macro is that it is easy to get started, but powerful and flexible enough for advanced needs. The user does not need to declare variables – their types are assigned automatically according to the data they store. The language also supports flow control, user-defined functions, I/O and error control. Functions can be called from other macros; this feature enables users to build their own libraries of Macro functions that can then be used by a larger user group.

This article outlines the key features and versatility of Metview Macro.

Overview of Metview Macro

The Metview Macro language provides an easy, powerful and comprehensive way for an analyst or researcher to manipulate and display meteorological data. It extends the use of Metview into an operational environment as it enables a user to write complex scripts that may be run with any desired periodicity. Metview has few runtime dependencies, thus making it ideal for running in an operational environment. This and the integrated access to MARS (Meteorological Archival and Retrieval System) archives makes Metview the ideal tool to run operational tasks for internal and external users of ECMWF's operational data. As described later, users can create and customise their visualisation interactively and then save it as a macro that can be executed in batch.

There are various ways to run a macro. It can be executed through the right-click menu of its icon on the GUI or executed within the Macro editor. Outside the GUI a script can be executed through the command *metview -b* followed by the name of the macro file and the macro's parameters. The latter is the way to run scripts in batch operationally, for example within SMS or as cron jobs.

To demonstrate the power of Metview Macro, consider the following example in Listing 1. To calculate and plot the difference between some point observations and an analysis field needs just four lines of code. The user does not need to worry about the conversion between formats and the interpolation of data values. If required, Metview directs such calculations to its support packages, such as Emoslib and Grib_API. The resulting plot is shown in Figure 1.

```
t2m_points = read("temperature_towns.gpt")
t2m_analysis = read("t2m_an.grib")
t2m_diff = t2m_points - t2m_analysis
plot(t2m_diff)
```

Listing 1 Example Macro visualising the difference between point observations and analysis field. Here 'grib' and 'gpt' are used as file extensions for the GRIB and Metview's Geopoints data formats respectively.

Key Macro features

Macro syntax and functions

Metview Macro offers all the facilities of a modern scripting language, for instance loops, if and case statements, and functions. As well as simple variable types (e.g. numbers, strings and lists), Macro has native variable types for commonly used meteorological data formats such as GRIB, BUFR, netCDF and ODB.

When used with the GUI, most interaction with Metview is performed via a rich set of icons that enable data retrieval, manipulation and plotting. For every icon, a corresponding Macro function exists; parameters are supplied via a set of parameter-value pairs whose syntax is based on the MARS language. Executing a *MARS Retrieval* icon and running the function *retrieve()* result in the same outcome.

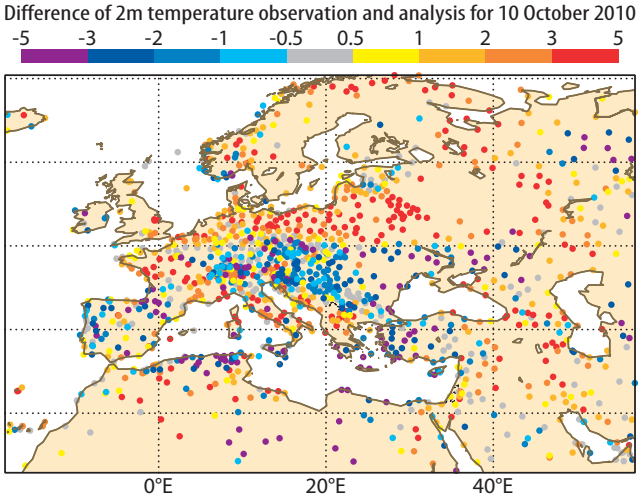

Figure 1 Plot resulting from Macro code in Listing 1. Additional to the listing, the differences between analysis and observation are coloured according to whether they are positive or negative.

In addition Metview Macro contains a large set of built-in functions that can be used for meteorological data processing. Macro also contains functionality to cache results, reducing the need to recalculate parts of the computation if the input data does not change. This can improve performance on repeated execution over the same data set. The time period of how long data is cached can be set in the Metview preferences.

Writing Macro code

The Metview user interface provides a Macro editor which not only offers syntax highlighting, but also the running and debugging of scripts interactively. While the editor in Metview 3 required the help of an additional external editor to offer extended functionality, the new Macro editor in Metview 4 is more powerful and supports all features expected from a modern code editor.

To allow users to quickly write Macro code, the Metview GUI offers features to generate code from the interactive user interface in two ways:

- Users who have generated their desired plot in the interactive plot window can use the 'Generate Macro' button (red punch card) to generate the corresponding macro code. In some cases of complex displays the resulting script may need some adjustments.
- Thanks to the direct mapping between desktop icons and macro icon-functions the user can drop an icon inside a macro editor. The result is the textual translation of the icon contents into a macro icon-function.

Figure 2 gives a snapshot of the Metview 4 macro editor.

Inlining Fortran and C/C++

The Macro language can be extended by the user with Fortran and C/C++ code. This ability extends immensely the scope of the macro language and enables the programmer to make efficient use of existing Fortran and C codes.

These programs are used in tasks that cannot be easily achieved by means of a Macro language function or combination of functions. Also, suitable code might already exist and the writing and testing of the same task in Macro language would simply consume precious time.

Building a Macro User Interface

Metview allows developers to build their own user interfaces to their scripts. These are useful to provide generality, meaning that the same Macro program used for a given task will be able to accept a variety of input parameters which will be provided via an icon editor window-like interface (in batch, parameters may be supplied on the command line). Listing 2 shows some sample code, and Figure 3 the resulting user interface.

```
c = slider (name    : "days",
            min     : 1,
            max     : 10,
            default : 5)
```

Listing 2 Macro code to generate a slider in a customised user interface.

Defining outputs

One major highlight of Metview 4 is the introduction of many more graphical output formats, due to the use of Magics++. Scripts run on the interactive GUI can make use of Metview 4's new interactive plot window or plot in new formats such as PDF, EPS, SVG and KML. These new options required a change in the way graphical output formats are defined in comparison to previous Metview versions. However, Metview 4 largely retains backwards compatibility with Metview 3's macro functions to export plots to files (`output()` and `setoutput()` functions). For more details see Box A.

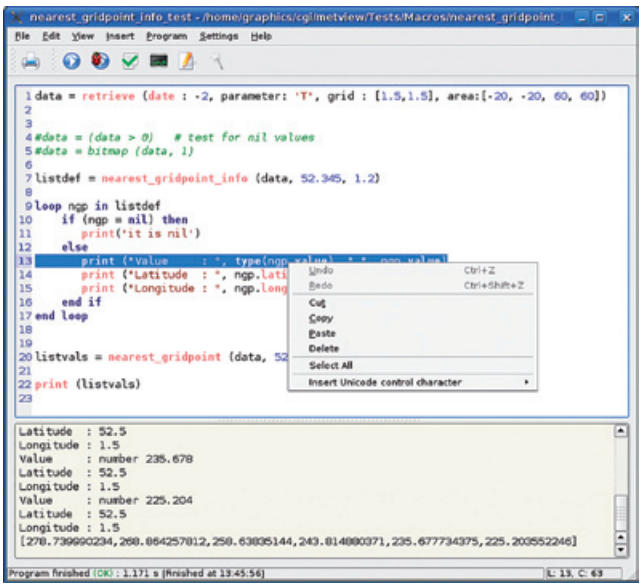

Figure 2 Snapshot of the Metview 4 Macro editor, showing syntax highlighting and debug output (bottom).

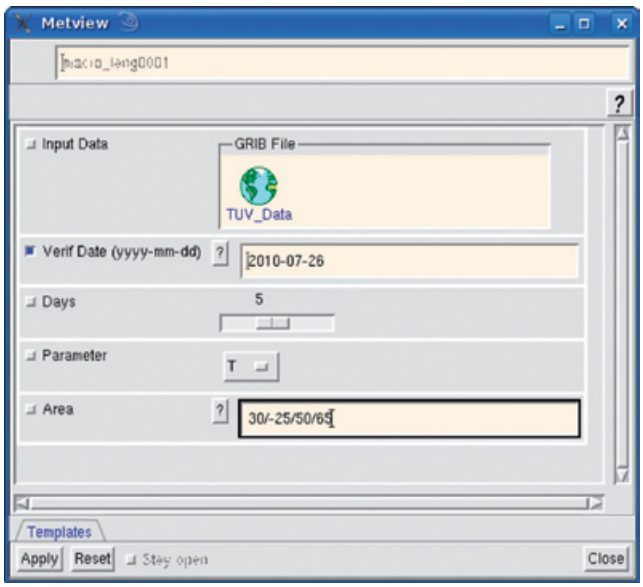

Figure 3 Snapshot of a user-defined user interface generated by a macro (see Listing 2 for a partial code listing).

Extensions to defining output formats in Metview 4

A

The following syntax is used to define a PostScript format in Metview 3:

```
ps = output(format    : "postscript",
            file_name : "plotfile.ps" )
```

Metview 4 has a new set of functions, for example:

```
ps  = ps_output ( output_name : "plotfile" )
kml = kml_output( output_name : "plotfile" )
svg = svg_output( output_name : "plotfile" )
```

Both syntaxes are valid in Metview 4. An extension is that setoutput() can take a list of several output definitions – in this case, Metview will generate its plot for all outputs. This can be significantly faster than running a macro multiple times (once for each output format). For instance:

```
setoutput([ps, kml, svg])
```

An alternative way to select which output formats will be generated is to give them directly to the `plot()` command:

```
plot([ps, kml, svg],…)
```

Any output formats given to the `plot()` command will override those given to `setoutput()`.

Optionally, within a macro the user can define specific output formats depending on the environment in which it is run:

```
# sets output destination according to
run-mode
if mode = "batch" then
     setoutput(ps_file)
else if mode = "visualise" then
     setoutput(screen)
end if
```

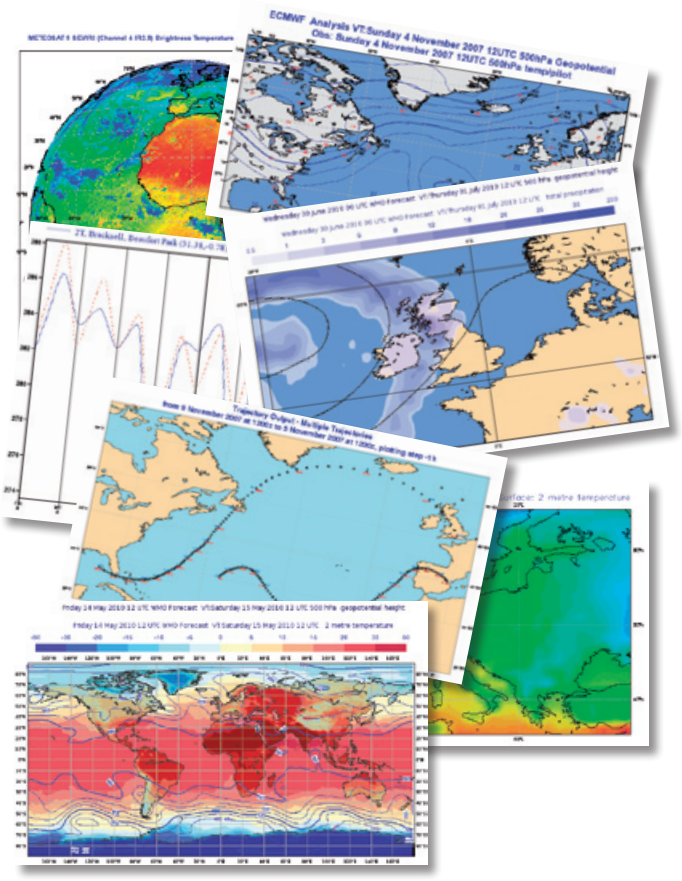

Figure 4 The user has all the functionality of the interactive graphical user interface plus a lot more.

Changes introduced in version 4.0

The new options to define outputs in Metview 4 are only the beginning of improvements to come for the Macro language (see Figure 4). Parameters are being cleaned up to remove those specific to MAGICS 6 and new ones added to access features in Magics++. Many issues in version 3 regarding performance and temporary files are being improved.

From version 4.0 onwards Metview's macro language handles missing values in its data in a more consistent and useful way. Previously, functions such as `integrate()` returned a 'missing value indicator' if all its input values were missing. This was not easy to test, and computations could use the result incorrectly without realising it. From now on all such functions return a `nil` variable when their inputs are invalid. Macros that do not test for this condition will fail if they try to use a `nil` variable in a computation. The following is an example code extract:

```
a = integrate(data)
if (a = nil) then
    fail ('Integration failed')
end if
```

The much improved installation scripts of Metview 4 will also allow for a batch only installation to reduce dependencies resulting from the GUI. This version is aimed for usage on operational servers.

Documentation, training and future developments

For users interested to find out more about Metview Macro there is full documentation of the language and available functions at:

http://www.ecmwf.int/publications/manuals/metview/documentation.html

The page also contains the training material from the annual Metview training course held at ECMWF, including tutorials and presentations.

The evolution of Metview's macro language will continue beyond the release of Metview 4.0. More built-in functions will be provided to support ECMWF tasks of observation handling and model developments. Metview's GUI and Macro editor will be extended to provide facilities to search for available macro functions and libraries.

User requests will of course continue to play an important role in improving the performance and reliability of Metview.

ECMWF Calendar 2011

January 6	Symposium on the occasion of Martin Miller's retirement
January 31 – February 4	Training Course – Use and interpretation of ECMWF products
February 7 – 11	Training Course – Use and interpretation of ECMWF products
February 14 – March 25	Training Course – Use of computing facilities
February 14 – 16	*Introduction to SMS/XCDP*
March 1 – 4	*GRIB API: library and tools*
March 7 – 11	*Introduction for new users/MARS*
March 14 – 15	*MAGICS*
March 16 – 18	*METVIEW*
March 21 – 25	*Use of supercomputing resources*
March 28 – May 25	Training Course – Numerical Weather Prediction
March 28 – April 1	*Numerical methods, adiabatic formulation of models and ocean wave forecasting*
April 4 – 14	*Parametrization of subgrid physical processes*
May 4 – 13	*Data assimilation and use of satellite data*
May 16 – 25	*Predictability, diagnostics and extended-range forecasting*
April 4	Joint ECMWF/ECOMET Workshop for Catalogue Contact Points
April 6	Advisory Committee for Data Policy (*12th Session*)
April 18 – 19	Policy Advisory Committee (*31st Session*)
April 27 – 28	Finance Committee (*88th Session*)
May 23 – 24	Security Representatives' Meeting
May 24 – 26	Computer Representatives' Meeting
June 8 – 10	Forecast Products – Users' Meeting
June 16 – 17	Council (*75th Session*)
June 21 – 24	Workshop on 'Treatment of model error in forecast models and data assimilation (THORPEX/WGNE)'
September 5 – 8	Seminar on 'Data assimilation for atmosphere and ocean'
September 26 – 28	Introduction to ECflow for SMS users
October 3 – 5	Scientific Advisory Committee (*40th Session*)
October 5 – 7	Technical Advisory Committee (*43rd Session*)
October 10 – 14	Training Course – Use and interpretation of ECMWF products for WMO Members
October 11 – 12	Finance Committee (*89th Session*)
October 12 – 13	Policy Advisory Committee (*32nd Session*)
October 17	Advisory Committee of Co-operating States (*17th Session*)
October 31 – November 4	13th Workshop on 'Meteorological operational systems'
November 8 – 10	Workshop on 'Diurnal cycles and the stable atmospheric boundary layer (GABLS)'
December 6 – 7	Council (*76th Session*)

ECMWF publications (see http://www.ecmwf.int/publications/)

Technical Memoranda

634 **Janssen, P.A.E.M.**: Ocean wave effects on the daily cycle in SST. *October 2010*

633 **Doblas-Reyes, F.J., M.A. Balmaseda, A. Weisheimer & T.N. Palmer**: Decadal climate prediction with the ECMWF coupled forecast system: Impact of ocean observations. *August 2010*

631 **Lu, Q., W. Bell, P. Bauer, N. Bormann & C. Peubey**: An initial evaluation of FY-3A satellite data. *July 2010*

ESA Contract Reports

WP-3300 contract 1-5576/07/NL/CB. **Di Michele, S. & P. Bauer**: Demonstration of monitoring. *August 2010*

WP-3200 contract 1-5576/07/NL/CB. **Janisková, M.**: Experimental assimilation of radar measurements. *August 2010*

WP-3100 contract 1-5576/07/NL/CB. **Janisková, M. & O. Stiller**: Development of strategies for radar and lidar data assimilation. *March 2010*

WP-2300 contract 1-5576/07/NL/CB. **Di Michele, S.**: Quality assessment of cloud screening, cloud analysis and cloud height assignment for atmospheric motion vectors. *April 2010*

WP-2200 contract 1-5576/07/NL/CB. **Morcrette, J.-J. & L. Jones**. Validation of aerosol parametrization – Representing a erosol processes in NWP. *November 2009*

WP-2100 contract 1-5576/07/NL/CB. **Forbes, R., M. Ahlgrimm, O. Stiller, S. Di Michele & J. Delanoe**: Validation of cloud parametrization. *December 2009*

WP-1000 contract 1-5576/07/NL/CB. **Di Michele, S., O. Stiller & R. Forbes**: Forward operator developments – errors and biases in representativity. *September 2009*

Index of past newsletter articles

This is a selection of articles published in the *ECMWF Newsletter* series during the last five years. Articles are arranged in date order within each subject category. Articles can be accessed on the ECMWF public website – www.ecmwf.int/publications/newsletter/index.html

Useful names and telephone numbers within ECMWF

Telephone

Telephone number of an individual at the Centre is:

International: +44 118 949 9 + three digit extension
UK: (0118) 949 9 + three digit extension
Internal: 2 + three digit extension

e.g. the Director-General's number:
+44 118 949 9001 (international),
(0118) 949 9001 (UK) and 2001 (internal).

E-mail

The e-mail address of an individual at the Centre is:
firstinitial.lastname@ecmwf.int

e.g. the Director-General's address: D.Marbouty@ecmwf.int

For double-barrelled names use a hyphen
e.g. J-N.Name-Name@ecmwf.int

ECMWF's public web site: http://www.ecmwf.int

	Ext
Director-General	
Dominique Marbouty	001
Deputy Director-General & Director of Operations	
Walter Zwieflhofer	003
Director of Research	
Erland Källén	005
Director of Administration	
Ute Dahremöller	007
Switchboard	
ECMWF switchboard	000
Advisory	
Internet mail addressed to Advisory@ecmwf.int	
Telefax (+44 118 986 9450, marked User Support)	
Computer Division	
Division Head	
Isabella Weger	050
Computer Operations Section Head	
Matthias Nethe	363
Networking and Computer Security Section Head	
Rémy Giraud	356
Servers and Desktops Section Head	
Richard Fisker	355
Systems Software Section Head	
Michael Hawkins	353
User Support Section Head	
Umberto Modigliani	382
User Support Staff	
Paul Dando	381
Dominique Lucas	386
Carsten Maaß	389
Pam Prior	384
Christian Weihrauch	380
Computer Operations	
Call Desk	303
Call Desk email: calldesk@ecmwf.int	
Console – Shift Leaders	803
Console fax number +44 118 949 9840	
Console email: newops@ecmwf.int	
Fault reporting – Call Desk	303
Registration – Call Desk	303
Service queries – Call Desk	303
Tape Requests – Tape Librarian	315

	Ext
Meteorological Division	
Division Head	
Erik Andersson	060
Meteorological Applications Section Head	
Alfred Hofstadler	400
Data and Services Section Head	
Baudouin Raoult	404
Graphics Section Head	
Stephan Siemen	375
Meteorological Operations Section Head	
David Richardson	420
Meteorological Analysts	
Antonio Garcia-Mendez	424
Anna Ghelli	425
Martin Janousek	460
Fernando Prates	421
Meteorological Operations Room	426
Data Division	
Division Head	
Jean-Noël Thépaut	030
Data Assimilation Section Head	
Lars Isaksen	852
Satellite Data Section Head	
Peter Bauer	080
Reanalysis Section Head	
Dick Dee	352
Probabilistic Forecasting & Diagnostics Division	
Division Head	
Tim Palmer	600
Predictability & Diagnostics Section Acting Head	
Roberto Buizza	653
Seasonal Forecasting Section Head	
Franco Molteni	108
Model Division	
Division Head	
Martin Miller	070
Numerical Aspects Section Head	
Agathe Untch	704
Physical Aspects Section Head	
Anton Beljaars	035
Ocean Waves Section Head	
Peter Janssen	116
GMES / MACC Coordinator	
Adrian Simmons	700
Education & Training (Acting)	
Sylvie Malardel	414
ECMWF library & documentation distribution	
Els Kooij-Connally	751